nature nanotechnology

Article

https://doi.org/10.1038/s41565-023-01359-6

Ectopic expression of a mechanosensitive channel confers spatiotemporal resolution to ultrasound stimulations of neurons for visual restoration

Received: 12 December 2021

Accepted: 13 February 2023

Published online: 3 April 2023

Check for updates

Sara Cadoni[1], Charlie Demené[2], Ignacio Alcala[1,7], Matthieu Provansal[1,7], Diep Nguyen[1], Dasha Nelidova[3], Guillaume Labernède[1], Jules Lubetzki[1], Ruben Goulet[1], Emma Burban[1], Julie Dégardin[1], Manuel Simonutti[1], Gregory Gauvain[1], Fabrice Arcizet[1], Olivier Marre[1], Deniz Dalkara[1], Botond Roska[3], José Alain Sahel[1,4,5,6], Mickael Tanter[2,7] & Serge Picaud[1,7]

Remote and precisely controlled activation of the brain is a fundamental challenge in the development of brain–machine interfaces for neurological treatments. Low-frequency ultrasound stimulation can be used to modulate neuronal activity deep in the brain, especially after expressing ultrasound-sensitive proteins. But so far, no study has described an ultrasound-mediated activation strategy whose spatiotemporal resolution and acoustic intensity are compatible with the mandatory needs of brain–machine interfaces, particularly for visual restoration. Here we combined the expression of large-conductance mechanosensitive ion channels with uncustomary high-frequency ultrasonic stimulation to activate retinal or cortical neurons over millisecond durations at a spatiotemporal resolution and acoustic energy deposit compatible with vision restoration. The in vivo sonogenetic activation of the visual cortex generated a behaviour associated with light perception. Our findings demonstrate that sonogenetics can deliver millisecond pattern presentations via an approach less invasive than current brain–machine interfaces for visual restoration.

Brain–machine interfaces (BMIs) based on multielectrode arrays (MEAs) have met with increasing success in peripheral sensory system rehabilitation strategies as well as for restoring hearing in the cochlea or sight in the retina[1,2]. The restoration of vision is the most demanding challenge for BMIs, as it ultimately requires the 13 Hz rate transmission of complex spatial patterns[3]. Although form perception can be achieved by epicortical or intracortical implants[4,5], the lack of long-term sustainability has intensified the search for the non-contact distant activation of neuronal circuits. Optogenetic therapy has provided an alternative, as demonstrated on the retina even at the clinical level[6].

[1]Sorbonne Université, INSERM, CNRS, Institut de la Vision, Paris, France. [2]Physics for Medicine Paris, INSERM, CNRS, École Supérieure de Physique et de Chimie Industrielles (ESPCI Paris), Paris Sciences et Lettres (PSL) Research University, Paris, France. [3]Institute of Molecular and Clinical Ophthalmology Basel, Basel, Switzerland. [4]Department of Ophthalmology, The University of Pittsburgh School of Medicine, Pittsburgh, PA, USA. [5]Department of Ophthalmology and Vitreo-Retinal Diseases, Fondation Ophtalmologique Rothschild, Paris, France. [6]Centre Hospitalier National d'Ophtalmologie des XV-XX, Paris, France. [7]These authors contributed equally: Ignacio Alcala, Matthieu Provansal, Mickael Tanter, Serge Picaud. e-mail: serge.picaud@inserm.fr

https://doi.org/10.1038/s41565-023-01359-6

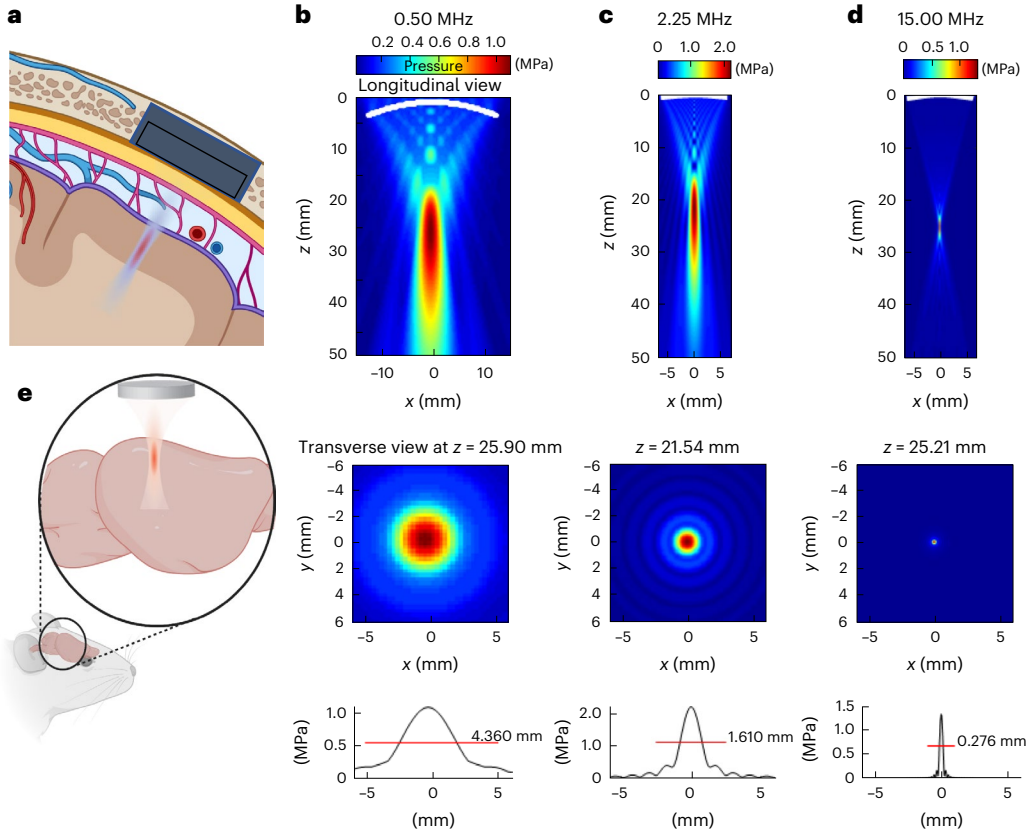

Fig. 1 | Sonogenetics using focused US beams for visual restoration through the intact dura mater: impact of ultrasonic transmission frequency. **a**, Concept of visual restoration with US matrix arrays implanted in a cranial window for the localized US neuromodulation of the primary visual cortex in humans. The US beam can be adaptively focused at different locations in the V1 cortex as it passes through the intact dura mater as well as subdural and subarachnoid spaces. **b**, Proof-of-concept setup used in this study for V1 sonogenetic activation in rodents, using a high-frequency focused transducer on a craniotomized mouse. **c**, Characterization of the radiated field for the 0.5 MHz transducer used in this study. A longitudinal view of the maximal pressure for a monochromatic acoustic field radiated at 0.5 MHz by the 25.40-mm-Ø, 31.75-mm-focus transducer (top). The maximum pressure is reached at 25.9 mm, slightly closer to the transducer than the geometric focal point, which is a documented effect. The transverse section of the maximum pressure field at depth $z = 25.9$ mm (middle). A one-dimensional profile of this transverse section giving the FWHM of the focal spot (4.36 mm at 0.5 MHz) (bottom). **d**, Same characterization for the 2.25 MHz 12.7-mm-Ø 25.4-mm-focus transducer. **e**, Same characterization for the 15 MHz 12.7-mm-Ø 25.4-mm-focus transducer. Note that the maximum pressure is reached very close to the geometric focus (25.21 mm versus 25.40 mm for the geometric focus) for this configuration. The FWHM of the focal spot is 0.276 mm. Panels **a** and **e** are created with Biorender.com.

Despite encouraging animal studies[7–9], approaches for the optical stimulation of the cortex are hindered by the dura mater and by brain scattering as well as the absorption of light requiring invasive light guides[10].

Ultrasound (US) waves could potentially overcome these limitations to achieve the non-contact neuromodulation of cortical and subcortical areas of the brains[11–17]. However, this neuromodulation requires a craniotomy (Fig. 1a) and the use of high US frequencies to reach the required spatial resolution. Switching from 0.5 MHz to 15.0 MHz would theoretically lead to a 30-fold improvement in resolution (Fig. 1c–e) and an ~27,000-fold improvement in neuromodulated volume. Unfortunately, most existing US neuromodulation strategies are restricted to low-frequency[15] or mid-range[18] transmissions resulting in poor spatial resolution (>3 mm) and/or long-lasting responses, whereas a high frequency of 30 MHz was reported to generate inhibitory neuromodulation[19]. Other attempts at high-frequency neuromodulation have resulted in higher levels of acoustic energy[20], with risks of thermal heating[21] and tissue damage[14].

Sonogenetic therapy has proposed to generate neuronal mechanosensitivity by the ectopic expression of US-sensitive proteins like the TRP1 ion channel[22], mechanosensitive ion channel of large conductance (MscL) (ref. 23) or auditory-sensing protein prestin[24] using AAV gene delivery to target specific cell populations[23,25,26], although without the spatiotemporal resolution compatible for vision restoration. A high temporal resolution was shown for MscL only in primary cultured hippocampal neurons with mutations enhancing its pressure sensitivity[27,28]—the G22S MscL mutant boosting US sensitivity of in vivo neurons[23].

Here we have investigated if we can use the MscL channel[29]: (1) to boost the neuronal sensitivity to US not only ex vivo but also in vivo, (2) to target a locally defined subset of neurons by gene therapy, (3) to induce responses with a temporal precision (millisecond time delay and recovery) sufficient for visual restoration and (4) to gain more than one order of magnitude in spatial resolution through the in vivo use of high-frequency US at low acoustic intensities to prevent adverse effects[20].

Sonogenetic activation on the ex vivo retina

Using the retina as an easily accessible part of the central nervous system, we specifically targeted MscL into rat retinal ganglion cells (RGCs), with in vivo intravitreous delivery by an adeno-associated vector (AAV) encoding the *mscL* gene from *Escherichia coli* in its wild-type (WT) form or with the G22S mutation[28]. An AAV2.7m8 (ref. 30) serotype vector was used to encode MscL fused to the red fluorescent

https://doi.org/10.1038/s41565-023-01359-6

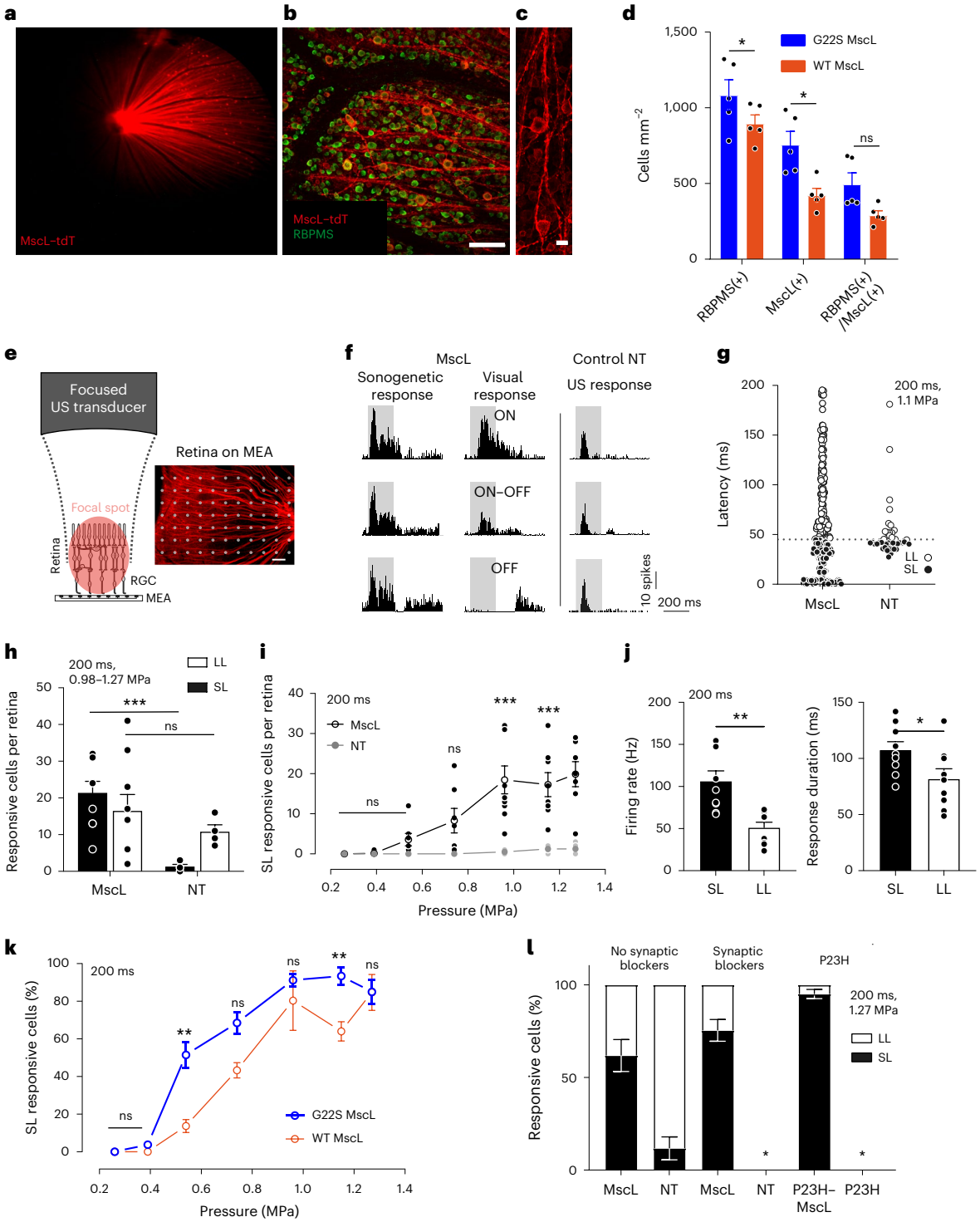

Fig. 2 | Sonogenetic therapy in rat RGCs. a, In vivo retinal fundus image showing MscL–tdTomato expression. **b**,**c**, Confocal stack projections across the RGC layer of a flat-mounted retina. **d**, Density of RBPMS-positive, MscL-positive and double-labelled cells ($n = 5$ WT MscL and G22S MscL retinas; $^{*}p = 0.0140$, for RBPMS(+); $^{*}p = 0.0465$ for RBPMS(+)/MscL(+), unpaired two-tailed t-test). **e**, Schematic of the experimental setup with an image of the retina on MEA electrodes. **f**, Representative peristimulus time histograms (PSTHs) for US or visual stimuli in MscL-transfected or NT RGCs (US stimuli, 15 MHz at 1.27 MPa). **g**, RGC response latencies to a 15 MHz US stimulus for MscL ($n = 300$ cells, 9 retinas) and NT retinas ($n = 41$ cells, 4 retinas). Dotted line, 45 ms latency threshold. **h**, Numbers of cells per retina responding to 15 MHz US stimuli (0.98–1.27 MPa) for MscL ($n = 9$ retinas) and NT ($n = 4$ retinas) with SL (<45 ms) or LL (>45 ms). $^{*}p = 0.0002$, unpaired two-tailed t-test. **i**, Mean numbers of SL-responding RGCs per retina following stimulation with US stimuli of increasing pressures for MscL ($n = 9$) and NT ($n = 4$) retinas. $^{***}p = 0.00008$, $^{***}p = 0.0010$, $^{***}p = 0.0008$, multiple unpaired two-tailed t-tests. **j**, Maximum firing rates and response durations (SL and LL RGCs from MscL retinas in response to US stimuli of increasing pressures (0.20–1.27 MPa)) ($n = 9$ retinas, $^{**}p = 0.0017$, $^{*}p = 0.0418$, unpaired two-tailed t-test). **k**, Percentages of SL RGC cells (normalized against the maximum number of responsive cells in each experiment) responding to US stimuli for WT MscL ($n = 3$ retinas) and G22S MscL ($n = 6$ retinas) retinas. $^{**}p = 0.0065$, $^{**}p = 0.0083$, multiple unpaired two-tailed t-tests. **l**, Ratios of RGCs responding to US stimulation with SL or LL for MscL and NT retinas ($n = 9$ retinas for MscL and 4 retinas for NT), following the application of a cocktail of synaptic blockers (CNQX-CPP-LAP4, $n = 3$ retinas for both MscL and NT) and for P23H retinas with and without MscL expression (for both, $n = 3$ retinas). *Conditions with no US-elicited cell responses. Data are presented as mean values ± standard error of the mean (s.e.m.). Scale bars, 100 µm (**b**), 20 µm (**c**), 200 µm (**e**).

protein tdTomato, under the control of the SNCG promoter to target the RGC population[31]. On the eye fundus, tdTomato fluorescence was detected in vivo (Fig. 2a). Its expression was restricted to RGCs, as indicated by their double labelling with a specific RGC antibody, RPBMS (Fig. 2b and Extended Data Fig. 1b). The expression of the MscL channel seemed to be concentrated at the cell membrane on the soma and axon (Fig. 2c and Extended Data Fig. 1) with 24% and 46% of RPBMS-positive cells expressing tdTomato for the WT MscL and G22S MscL proteins, respectively (Fig. 2d).

During the ex vivo recordings of the MscL-expressing retina (Fig. 2e), RGCs displayed strong and sustained ON spiking responses to focused 15 MHz US stimulation (Fig. 2f (left)) irrespective of their ON or OFF responses to light (Extended Data Fig. 2a). Many RGCs presented responses with very short latencies (SLs), namely, 12.2 ± 2.5 ms (Fig. 2f (left)), but some had long latencies (LLs) (Fig. 2g). By contrast, non-transfected (NT) retina displayed only LL responses, that is, 50.4 ± 4.2 ms (Fig. 2f (right) and Fig. 2g). Synaptic blockers (CNQX-LAP4-CPP) abolished US responses in NT retinas but not in MscL-transfected retinas, in which they decreased the number of LL US responses (LL denotes latency of more than 45 ms; Fig. 2l and Extended Data Fig. 2c,d). This observation suggests that responses in NT retinas originate upstream from RGCs, as previously reported[32]. This conclusion was supported by the absence of US response in the retinas of NT blind P23H rats having lost photoreceptors whereas transfected P23H showed a majority of SL responses (<45 ms) (Fig. 2l and Extended Data Fig. 2c,d). The geometric-mean latencies in MscL-tested groups were very different from those for the NT retina, especially in the blind P23H retina (Extended Data Fig. 2c), but the cumulative distribution of latencies further highlighted these differences (Extended Data Fig. 2d). These results suggested a natural mechanosensitivity in photoreceptors highly reminiscent of that of auditive cells in agreement with the expression of Usher proteins in both sensory cells. These proteins are known for generating the auditory mechanotransduction and probably the phototropism of photoreceptors underlying the Stiles Crawford effect[33].

MscL expression decreased latency and increased the mean number of cells per retina responding to US (Fig. 2h). SL-responding cells expressing MscL were sensitive at much lower US pressures than NT cells and their number increased with the US pressure (Fig. 2i). SL US responses also involved higher firing rates and were more sustained than LL US responses (Fig. 2j). Moreover, we observed that the G22S mutation further enhanced the sensitivity of SL RGCs to lower US pressures (Fig. 2k and Extended Data Fig. 1b). We subsequently restricted our analyses to SL US responses (<45 ms). Neurons responded even to very short stimulation durations (10 ms), with responses showing a fast return to the control level of activity (Fig. 3a). US response durations were correlated with the stimulus duration, although a reduction in the firing rate occurred for longer stimuli (>100 ms) (Fig. 3c,d). Using different stimulus repetition rates, RGCs were able to follow rhythms up to a 10 Hz frequency (Fig. 3b–e). The Fano factor indicated that the response had low variability in the spike count and possibly high information content (Fig. 3c–e).

We then investigated whether different US frequencies (0.50, 2.25 and 15.00 MHz) affected the spatial resolution of the response, in accordance with the measured US pressure fields (Extended Data Fig. 3). Transducers were designed with a similar focal distance and numerical aperture, for the transmission of focused beams over different frequency ranges (0.50, 2.25 and 15.00 MHz, corresponding to wavelengths of 3.0, 0.7 and 0.1 mm, respectively) (Fig. 1c–e). Features of responses evoked by the different US frequencies were found to be similar (Extended Data Fig. 2e,f), although increasing the frequency from 0.5 MHz (typical of neuromodulation) (Fig. 1c) to 15.0 MHz (Fig. 1e) reduced the focal spot by a factor of ~4,100 with our transducers. Cells responding to US were widespread over the recorded area for 0.50 and 2.25 MHz, but appeared to be more confined for 15.00 MHz (Fig. 3f), despite similar acoustic parameters (100 ms at 1.1 and 1.3 MPa) for the 2.25 MHz and 15.00 MHz beams. The acoustic pressure at 0.5 MHz was lower (0.5 MPa) due to electric-power limitation of our electronics. The spatial dispersion of activated cells decreased significantly from 1.48 ± 0.12 mm and 1.30 ± 0.18 mm at 0.50 MHz and 2.25 MHz, respectively, to 0.59 ± 0.03 mm at 15.00 MHz (Fig. 3g). This spatial dispersion was consistent with the size of the measured US pressure fields (Fig. 1c–e); for the 0.50 MHz transducer, the focal spot was much larger than the MEA chip. The density of activated cells increased significantly with increasing US frequency but on a smaller area (Fig. 3h). US stimulation is more effective at higher frequencies, because lower acoustic power values are required to activate an equivalent number of cells. Indeed, even if the acoustic intensities at 2.25 and 15.00 MHz were fairly similar, the acoustic power delivered was almost two orders of magnitude lower at 15.00 MHz (0.03 W) than at 2.25 MHz (0.82 W). At 15.00 MHz, moving the focal spot of the US probe above the retina triggered a shift in the area of responding cells (Fig. 3i). The response centre was found to move in accordance with the displacement of the US transducer (Fig. 3j). These results demonstrate that our sonogenetic therapy approach can efficiently activate neurons with a millisecond and submillimetre precision.

Spatiotemporal resolution in vivo on the visual cortex

We investigated whether this approach could also be applied to the brain in vivo through a cranial window (Fig. 1a,b). As the G22S mutation enhanced the US sensitivity of RGCs ex vivo, we expressed G22S MscL in cortical neurons of the primary visual cortex (V1) in rats. We injected AAV9.7m8 encoding the G22S MscL channel fused to tdTomato under the control of the neuron-specific CamKII promoter into V1. The tdTomato fluorescence was detected in the brain (Fig. 4a) and in cortical slices, particularly in layer 4 (Fig. 4b). Staining with an anti-NeuN antibody showed that 33.4% of cortical neurons in the transfected area expressed tdTomato (Fig. 4c).

To measure the responses to 15 MHz US stimulations, we placed a micro-electrocorticography (μEcoG) electrode array on the cortical surface of V1 (Fig. 4d). In NT animals, no US-evoked signal was recorded (Fig. 4e (right), $n = 3$ rats), whereas in V1 expressing G22S MscL, the US stimulation of the cortical surface elicited large negative μEcoG potentials (Fig. 4e (middle), $n = 6$ rats). These US-evoked negative deflections were different from the recorded visual-evoked potentials (Fig. 4e (left)). Amplitudes and durations of the US responses were clearly related to the duration of US stimulations (Fig. 4f,h) and US pressures (Fig. 4g). V1 cortical responses were again able to follow a repetition rate of up to 13 Hz (Fig. 4i) even if the peak amplitude slightly decreased for increasing stimulation frequencies.

The peak depolarization of each channel was measured and linearly interpolated to build pseudocolour activation maps showing sizes of the US-responding cortical area dependent on the US pressure from 0.26 MPa (0.58 ± 0.17 mm^2, $n = 6$ rats) to 1.27 MPa (1.41 ± 0.23 mm^2, $n = 5$ rats) (Fig. 4j–l). When the US probe was moved laterally, the source of the generated neuronal activity moved in a similar direction (Fig. 4k). The spatial location of the evoked potentials moved by 0.29 mm (±0.09 mm, $n = 6$ rats) from the previous location (Fig. 4m and Extended Data Fig. 5), even though we moved the US transducer in 0.40 mm steps. This discrepancy between the displacement of the activated area and movement of the transducer was certainly related to the 0.3 mm discrete spatial pitch distribution of the electrodes and the lateral spread of activity in the circuit. These results suggest that our approach to sonogenetic therapy could yield a spatial resolution of within 400 μm for stimulations at 15 MHz, the focal spot of our 15 MHz transducer being 276 μm wide (Fig. 1d). This opens up the possibility of targeting small areas (down to 0.58 mm^2 for 0.26 MPa), depending on the pressure level. These very localized US-evoked responses, their dependence on the position of the US probe and their SLs confirmed

https://doi.org/10.1038/s41565-023-01359-6

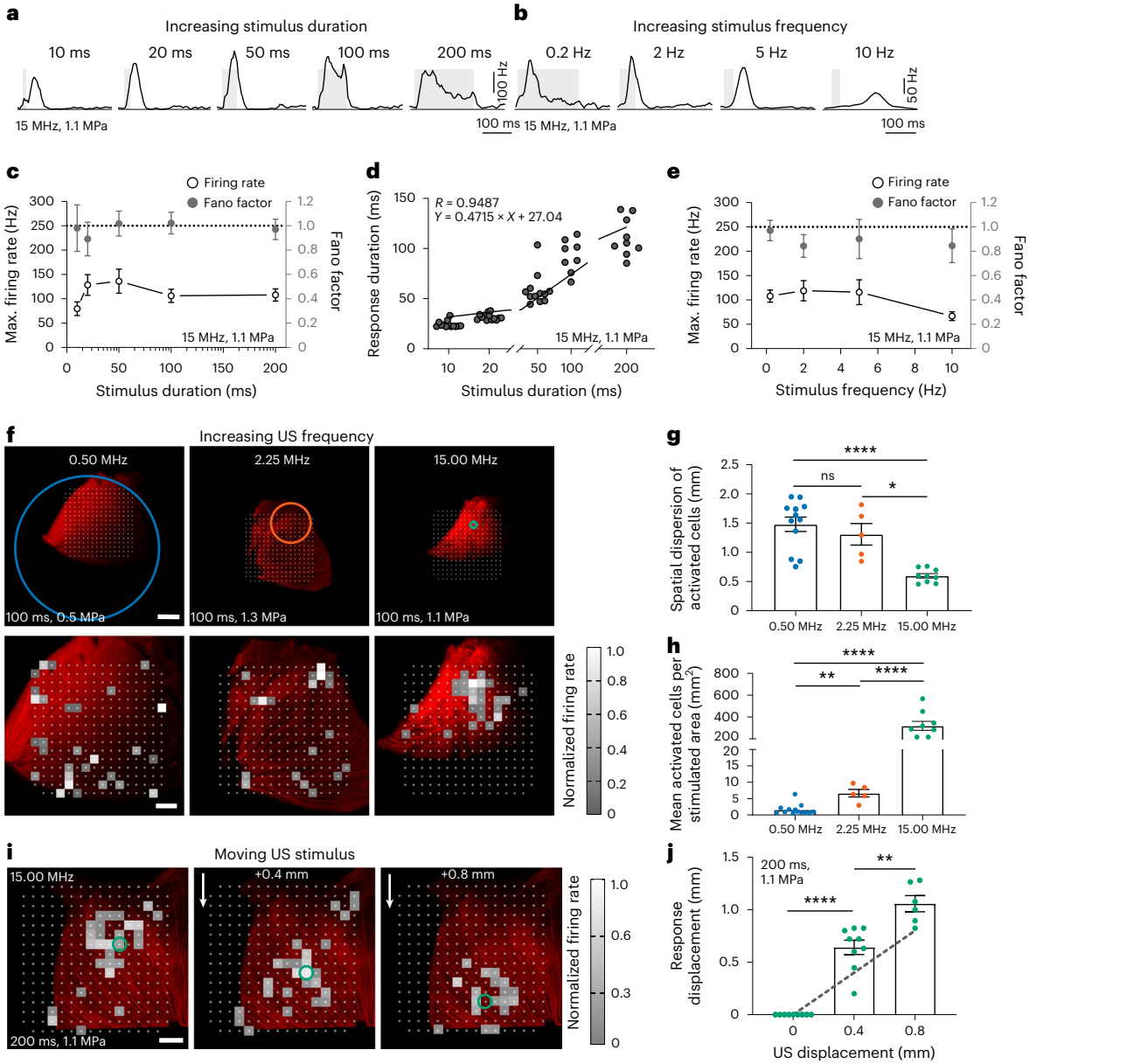

Fig. 3 | Spatiotemporal properties of sonogenetic retinal responses. **a**,**b**, Spike density functions of two RGCs from the MscL retina for 15 MHz stimulus durations and repetition frequencies (0.5 Hz repetition rate (**a**); 10, 20, 50 and 200 ms durations (**b**)). **c**, Maximum firing rates for different 15 MHz stimulus durations and mean Fano factor values for all the cells (10–20 ms, $n = 8$ retinas; 50–200 ms, $n = 9$ retinas). **d**, Correlation between response duration and stimulus duration ($n = 9$ retinas). **e**, Maximum firing rates for different stimulus repetition frequencies and mean Fano factor values for all the cells (0.2–2.0 Hz, $n = 9$ retinas; 5.0–10.0 Hz, $n = 8$ retinas). **f**, Retinas on an MEA chip and the corresponding size of the incident US pressure beam (the circles represent the FWHM and are centred on the estimated centre of the response) for 0.50, 2.25 and 15.00 MHz (top). The corresponding activation maps representing the normalized firing rates of the cells following US stimulation (bottom). Each square box represents an electrode with at least one US-activated cell. **g**,**h**, Spatial dispersions of activated cells (**g**) and ratios of the number of activated cells to the stimulated area for the three US frequencies (**h**); $^{****}p = 0.00002$ (**g**), $p = 0.00006$ (15.00 versus 2.25 MHz) and $p = 0.00005$ (15.00 versus 0.50 MHz) (**h**); $^{**}p = 0.0008$, $^{*}p = 0.0169$, unpaired two-tailed t-test. Here $n = 12$ retinas for 0.50 MHz (0.29–0.68 MPa), $n = 5$ retinas for 2.25 MHz (1.11–1.62 MPa) and $n = 9$ retinas for 15.00 MHz (1.12–1.27 MPa). **i**, Heat maps showing activated cells in the MscL retina following displacements (0.4 and 0.8 mm) of the US transducer. The circles represent the estimated centre of the response. **j**, Relative displacements of the centre of the response following the displacement of the 15 MHz US transducer. $^{****}p = 0.00001$, $^{**}p = 0.0018$, unpaired two-tailed t-test. Here $n = 9$, 9 and 6 positions for 4, 4 and 2 retinas for displacements of 0, 0.40 ± 0.20 and 0.80 ± 0.18 mm (s.d.), respectively. The grey dotted line represents the theoretical displacement. Data are presented as mean values ± s.e.m. Scale bars, 1.0 mm (**f**, top); 0.5 mm (**f** (bottom) and **i**).

that they were due to the activation of G22S MscL-expressing neurons and not to an indirect response related to auditory activation, as suggested previously[34,35].

When recording with penetrating electrode arrays (Fig. 4d), V1 neurons expressing G22S MscL generated sustained responses even to 10-ms-long 15 MHz US stimuli (Fig. 5a) with latencies shorter than 10 ms (5.10 ± 0.62 ms, $n = 27$ cells) (Fig. 5b), consistent with direct US activation. Responding neurons were recorded at various cortical depths, ranging from 100 µm to 1.00 mm (Fig. 5c), the focal spot diameter of the US probe being 3.75 mm in the x–z plane. Deep neurons reliably responded to the stimuli of decreasing duration, from 50 ms to 10 ms, with similar firing rates, whereas longer stimuli induced responses in

https://doi.org/10.1038/s41565-023-01359-6

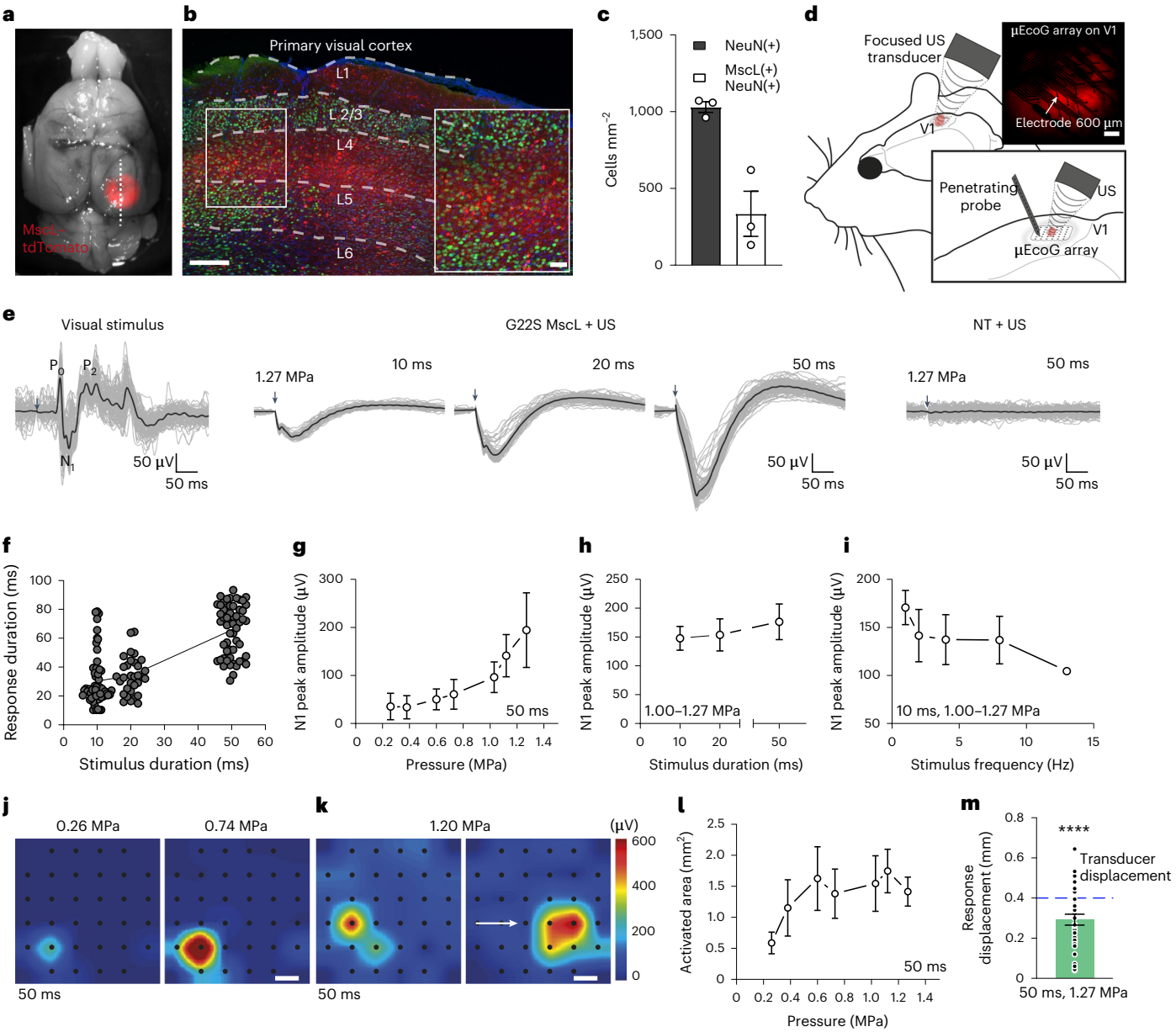

Fig. 4 | Spatial resolution of in vivo sonogenetic therapy in V1 cortical neurons. **a**, Image of a rat brain expressing G22S MscL–tdTomato (red) in V1. **b**, Confocal stack projection of a sagittal brain slice expressing G22S MscL–tdTomato (red) and labelled with anti-NeuN antibody (green) and DAPI (blue). The layers of V1 are delineated by the dashed white lines. Magnification of layer 4 of V1 (lower right). **c**, Densities of NeuN-positive, MscL-positive and double-labelled cells for three brain slices. **d**, Schematic of the setup used for in vivo electrophysiological recordings and US stimulation. µEcoG electrode array placed on V1 of an MscL-transfected rat (top right). **e**, Visual-evoked cortical potentials in response to a 100 ms flash (left). Sonogenetic-evoked potentials for 15 MHz US stimuli of various durations (middle). Absence of US responses in an NT rat to a 15 MHz stimulus (right). The black traces represent the mean evoked potentials over 100 trials, individually illustrated by the grey traces. The black arrows indicate the stimulus onsets. **f**, Duration of sonogenetic µEcog responses for the stimuli of different durations (10 ms, $n = 58$ trials; 20 ms, $n = 32$ trials; 50 ms, $n = 56$ trials on 6 animals). **g**–**i**, N1 peak amplitudes for increasing US pressure (**g**), increasing duration (**h**) and increasing frequency (**i**) ($n = 6$ rats). **j**,**k**, Pseudocolour activation maps for the stimuli of increasing US pressure (**j**) and for a horizontal displacement of the US transducer by 0.8 mm (**k**) (the arrow indicates the direction of displacement). Each black dot represents an electrode of the array. The colour bar represents the N1 peak amplitude in microvolts. **l**, Mean activated areas for various US pressure values ($n = 6$ animals). **m**, Relative displacement of the activation centre to the previous position following movement of the US transducer by 0.4 mm. Here $p = 1 \times 10^{-12}$, one-sample two-tailed t-test, $n = 37$ positions on 6 animals (mean, 0.29 ± 0.16 mm (s.d.)). Data are presented as mean values ± s.e.m. Scale bars, 200 and 50 µm (**b**); 300 µm (**j** and **k**).

a broader population of neurons (Fig. 5d–e). To investigate if a US pattern could be applied for visual restoration at a refreshing rate of up to 13 Hz, we progressively increased the sequence of stimuli. Cortical neurons were able to generate distinct responses to each US stimulus up to a 13 Hz repetition rate (Fig. 5f), but the number of responding cells decreased with increasing stimulus frequency (Fig. 5g). No major tissue temperature increase is expected even at this stimulation rate (Extended Data Fig. 4).

Behavioural response to the sonogenetic stimulation of the visual cortex

To define if the US-elicited synchronous activation of MscL-expressing excitatory cortical neurons can induce light perception, we assessed the mouse behaviour during an associative learning test including 15 MHz US stimulation of V1 in G22S MscL-transfected ($n = 14$) and NT ($n = 9$) animals (Fig. 6 and Extended Data Fig. 6). Mice subjected to water deprivation were trained to associate the visible-light stimulation of

https://doi.org/10.1038/s41565-023-01359-6

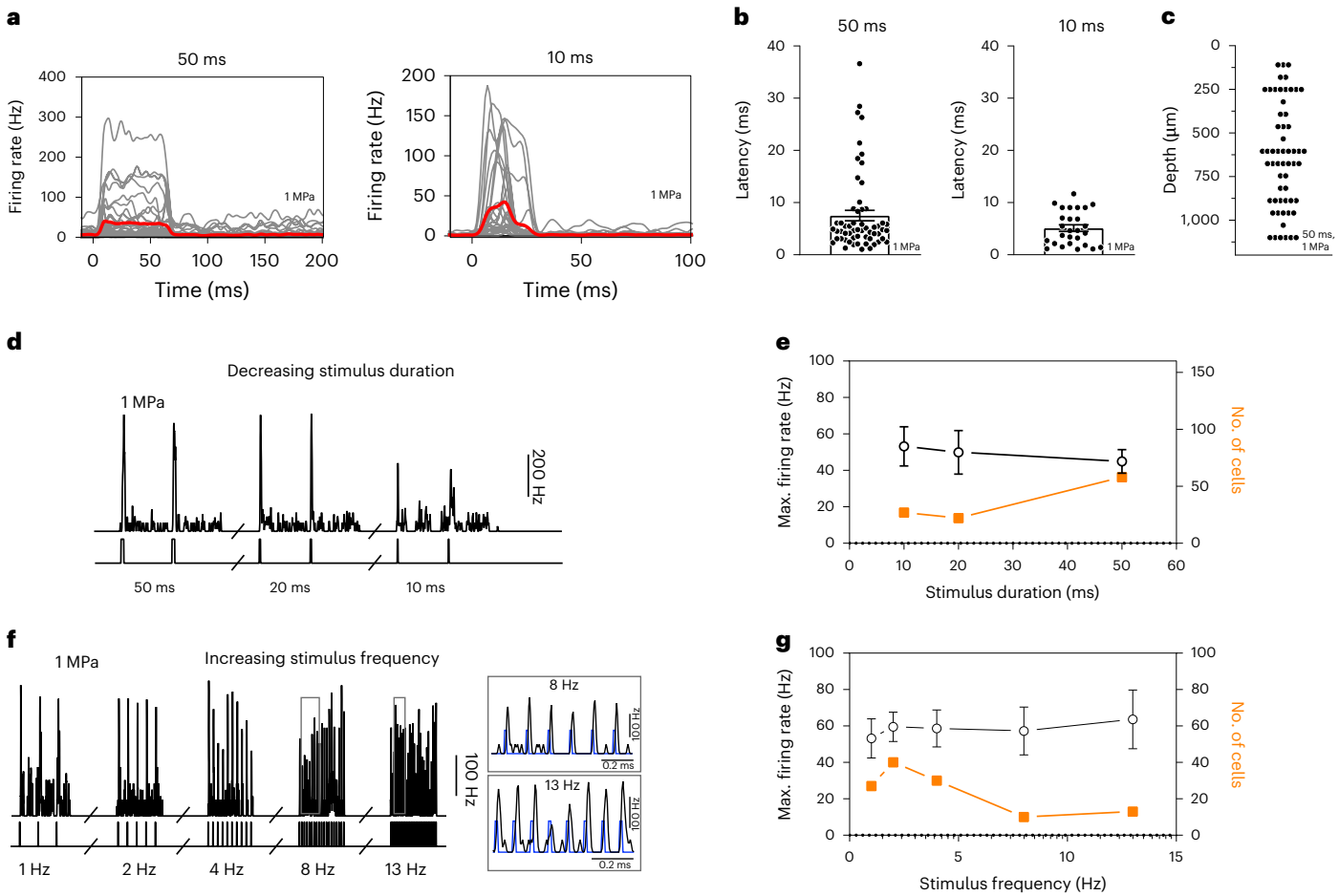

Fig. 5 | Temporal resolution of in vivo sonogenetic cortical activation. **a**, Spike density functions (SDF) of 58 and 27 neurons recorded with a penetrating MEA in MscL-transfected rats following US stimulation for 50 and 10 ms (red, mean trace; grey, individual cells). **b**, Response latencies following 50 and 10 ms of US stimuli (50 ms, $n = 58$ cells, mean of 7.5 ± 7.6 ms (s.d.), 7 rats; 10 ms, $n = 27$ cells, mean of 5.1 ± 3.2 ms (s.d.), 5 rats). **c**, Depth of US-responding cells ($n = 58$) in MscL-expressing rats ($n = 7$). **d**, Instantaneous SDF of responses to US stimuli of different durations (1 Hz stimulus repetition frequency). **e**, Maximum firing rates ($n = 27$, 22 and 58 cells; s.d., 55.8, 56.2 and 49.8 ms for 10, 20 and 50 ms stimulation, respectively) and numbers of activated neurons on US stimulations of different durations (US pressure, 1 MPa). **f**, Instantaneous SDF of responses to US stimuli of different repetition frequencies (10 ms stimulus duration). **g**, Mean maximum firing rate and number of activated neurons on US stimulation at different stimulus repetition frequencies (10 ms, 1 MPa, $n = 27, 40, 30, 10, 13$ cells; s.d., 55.8, 50.8, 55.7, 41.5, 58.2 Hz). Data are presented as mean values ± s.e.m.

one eye with a water reward (Fig. 6a)[36]. This task was learned within four days, as indicated by the increasing success rate during this period, from 30.9 ± 17.9% (standard deviation (s.d.)) to 86.2 ± 14.1% (s.d.) for G22S MscL-transfected mice (Fig. 6b). The success rate was determined by assessing the occurrence of an anticipatory lick between the light onset and the release of water reward 500 ms later (Fig. 6a). Only mice reaching a 60% success rate on the fourth day were retained for this analysis, and sessions showing a compulsive licking rate were excluded. Following cortical US stimulation on day 5, G22S MscL-transfected mice achieved a success rate of 69.3 ± 25.4% (s.d.), the difference of which showed no statistical difference with the success rate following light stimulation (LS) on day 4 (Fig. 6b). After a pause during the weekend (days 6–7), the animals retained the task, their success rates showing no statistically significant differences with the one following LS (Fig. 6b). By contrast, in NT animals, the success rate following the US stimulation of their visual cortex dropped to 38.1 ± 18.5% (s.d.), and the difference with the success rate following LS on the fourth day was highly significant ($p < 0.0001$) (Fig. 6d and Extended Data Fig. 6). In the AAV-injected mice, we found that the latency of the first anticipatory lick was shorter for sonogenetic stimulation (187.1 ± 37.3 ms; $n = 14$ (s.d.)) than for stimulation with a light flash (265.9 ± 46.5 ms; $n = 23$ (s.d.)) (Fig. 6c and Extended Data Fig. 6d). This SL for the US response is consistent with the faster activation of cortical neurons for sonogenetic stimulation than for LS of the eye (Fig. 4e). In transfected mice, success rates increased with pressure (Fig. 6d), suggesting a brighter and/or a larger US-elicited percept with a greater US pressure, as described with increasing currents in human patients[4]. Interestingly, the licking frequency during 500 ms before delivery of the water reward also increased with US pressure (Fig. 6e). These results suggest that the sonogenetic stimulation of the visual cortex generates a perception in mice that is probably associated with a visual perception, although more complex visual behaviours (as form discrimination) would be required for a demonstration.

Safety issues

Our sonogenetic approach greatly decreased the US pressure required for the activation of RGCs and V1 cortical neurons with stimulation sequences remaining below FDA safety limits (510(k), Track 3) for US imaging (for example, for a 10 ms US stimulus of 0.6 MPa, the non-derated spatial peak temporal peak intensity (Isptp) is 12.00 W cm^{-2} and the non-derated Ispta value is 0.12 W cm^{-2}). These very low acoustic pressures and acoustic intensities prevent tissue damage, as they are similar to those that have been widely used in clinical diagnostic imaging for decades[37]. Moreover, the simulations of US-induced heating

https://doi.org/10.1038/s41565-023-01359-6

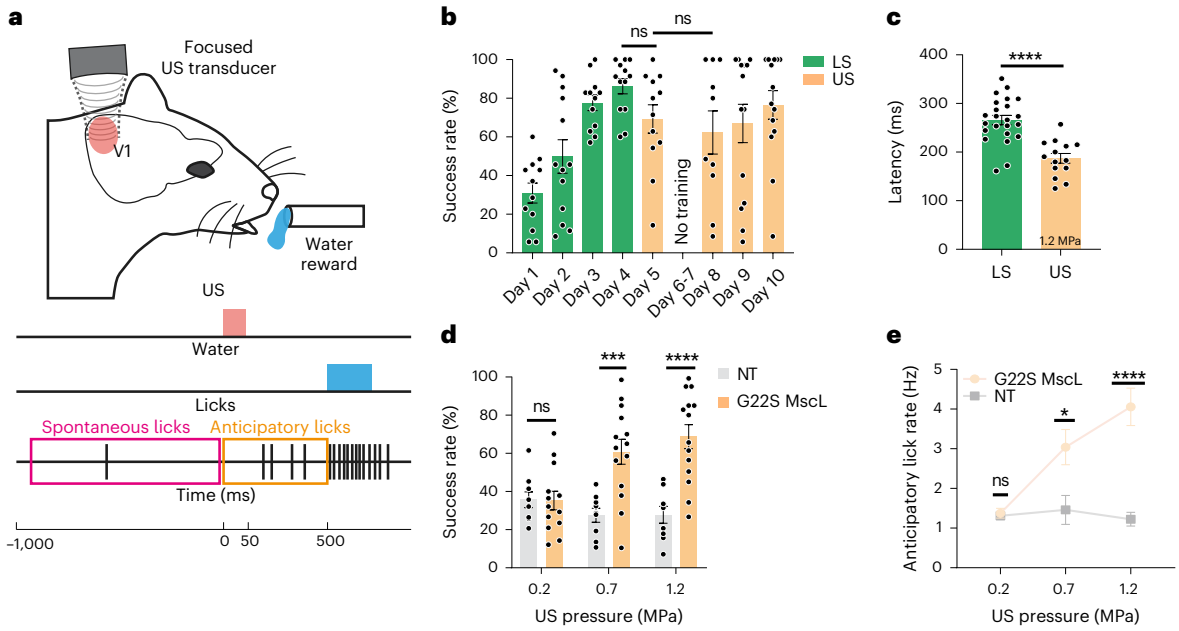

Fig. 6 | Behavioural response induced by the sonogenetic activation of the V1 cortex in mice following associative visual training. a, Schematic of the behavioural task performed by mice. Water-restricted animals trained in an associative learning paradigm for light stimulation (LS) with a water reward are subjected to either an LS of the eye (days 1–4) or the US stimulation of V1 at 15 MHz (days 5 and 8–10). **b**, Mean rates of successful trials for 4 days of training during the learning of association between LS (green, 50 ms) and water reward followed by US stimulation (orange, 1.2 MPa) for G22S MscL-transfected mice (between day 4 of LS and day 5 of US; 50 ms at 1.2 MPa; ns, $p = 0.0570$). Between day 5 of US and day 8 of US, 50 ms at 1.2 MPa; ns, $p = 0.6079$, two-tailed unpaired *t*-test; mean, 30.9%, 49.9%, 77.6%, 86.2%, 69.3%, 62.3%, 66.9%, 76.5%; s.d., 17.9%, 31.2%, 13.9%, 14.1%, 25.4%, 35.4%, 37.1%, 27.7%; $n = 14$ animals. **c**, Mean times to first lick after light (50 ms) and US stimulation (50 ms at 1.2 MPa) (****$p = 0.0000290$, two-tailed unpaired *t*-test, $n = 23$ and $n = 14$ animals; mean, 265.9, 187.1 ms and s.d., 46.5, 37.3 ms for LS and US, respectively). **d**, Mean rates of successful trials over 4 days of US stimulation for NT and G22S MscL-transfected mice, following 50 ms of US stimulation at increasing US pressures (ns $p = 0.9452$, ***$p = 0.0003$, ****$p = 0.0000296$, two-tailed unpaired *t*-test, for 0.2, 0.7 and 1.2 MPa, respectively; $n = 14$ animals; mean, 35.2%, 60.8%, 68.7% and s.d., 17.5%, 24.4%, 23.6% for G22S MscL; $n = 9$ animals; mean, 35.7%, 27.5%, 27.8% and s.d., 12.4%, 11.0%, 13.2% for NT). **e**, Session anticipatory lick rates for NT and G22S MscL-transfected mice at increasing US pressures (ns $p = 0.6934$, *$p = 0.0119$, ****$p = 0.0000340$, two-tailed unpaired *t*-test, for 0.2, 0.7 and 1.2 MPa, respectively; $n = 14$ animals; mean: 1.4, 3.0, 4.1 and s.d., 0.4, 1.7, 1.8 Hz for G22S MscL and $n = 9$ animals; mean, 1.3, 1.4, 1.2 and s.d., 0.3, 1.1, 0.5 Hz for NT). Data are presented as mean values ± s.e.m.

in brain tissue revealed that typical US parameters (that is, 20 ms at 1.27 MPa) (Fig. 4e–h) increased the local temperature by an estimated 0.12 °C, with even high repetition rates (up to 13 Hz), leading to a moderate temperature increase (<0.30 °C) (Extended Data Fig. 4c–f). These low temperature fluctuations (corresponding to 'worst-case' scenarios as we used non-derated US parameters) and stimulation sequences compliant with FDA limits suggest that our approach had no toxic side effects and that US-elicited responses were not temperature driven and were therefore probably mediated by the mechanical activation of MscL channels by US. The fact that acoustic intensities and pressures used here remained far below the FDA requirements for conventional ultrasonic imaging in clinics (https://www.fda.gov/media/71100/download) and generated very low temperature increase in comparison with thermal damaging effects[38] raises high hopes for a smooth clinical translation. Moreover, a very recent safety study[19] demonstrated an absence of brain tissue damage using high-frequency activation at ten times higher acoustic intensities (continuous insonication at 11.80 W cm^{-2} compared with our worst-case spatial peak temporal average intensity (Ispta) of 1.56 W cm^{-2} for repeated stimulations at 13 Hz rate).

Conclusions

The development of remotely controlled cortical and subcortical deep neuronal stimulation techniques is of considerable interest for the treatment of diverse neurological diseases and sensory handicaps. Most previous sonogenetic studies focused on the use of low-frequency US[22–24] as in the recent demonstration of MscL-based sonogenetic activation in mouse brain[23]. However, such low-frequency US waves lead to limited centimetre spatial resolutions (~5 × 5 × 45 mm^3) and an uncontrolled spatial-beam distribution. An alternative approach to spatially containing US stimulations involves the use of higher US frequencies, but this was thought to demand higher energy levels, exceeding safety limits and favouring tissue damage[20]. The bacterial MscL channel has been reported to sensitize neurons to US[23,27,28] and to lower the pressure for neuronal activation, but its use for high-spatiotemporal-resolution sonogenetic stimulation has yet to be shown to be effective in vivo. We here showed that that US activation of G22S MscL expressed in retinal or cortical neurons resulted in responses with millisecond latencies and a spatial resolution of at least 400 µm in the x–y plane at 15 MHz frequency. The subsequent neuronal activation throughout the depth of the visual cortex (Fig. 5n–p) led to a behavioural motor response, suggesting light perception by the animal. These sonogenetic responses were genuinely related to MscL expression, as they were not observed in NT animals. Following previous demonstrations that the MscL channel is a suitable sonogenetic actuator[23,27,28], we provide further evidence that the MscL channel has appropriate kinetics for the activation of neurons at a precise spatiotemporal resolution both in situ and in vivo.

The temporal precision of sonogenetics is lower than that achieved with optogenetics (>40 Hz) by the fastest opsins[39] and ChrimsonR (ref. 40), which can successfully restore vision at the retinal level in patients[6]. MscL only follows a 13 Hz frequency in vivo, which is in the same range as the 5–20 Hz achieved in vivo by the very sensitive opsin, ChRmine (ref. 41), a frequency range probably sufficient for vision[3]. The discovery of ChRmine has enabled investigators to stimulate deep into the rodent brain even from above the skull[41]. Future studies will have to examine the spatial resolution of this approach and how it compares to sonogenetics. As for all the gene therapies in non-dividing

cells, both optogenetic and sonogenetic therapies are expected to be lifelong lasting as indicated by gene therapy in congenital Leber congenital amaurosis, although it did not stop the ongoing degeneration of photoreceptors in patients[32].

Restoration of form vision at the cortical level was previously achieved with 0.5 to 1.0 mm surface electrodes spaced more than 1.0 mm apart[5] or with 1.5-mm-long penetrating electrodes spaced 400 µm apart[4]. The spatial resolution of the proposed sonogenetic therapy, therefore, appears to be compatible with the cortical restoration of form vision but with a remote non-contact device. To preserve this spatiotemporal resolution, the US stimulator will require to be placed directly above the dura mater or above a US transparent artificial skull[42]. At 15 MHz, the typical penetration depth with negligible heating is 20 mm. Moreover, the resolution of the approach could be increased by using gene therapy to drive the expression in specific cell populations and cell compartments[31,43]. Further studies are required to generate an interface for coding visual information into US patterns transmitted by an ultrasonic matrix array onto the visual cortex at a video rate. To reduce the US load, visual restoration can take advantage of an event-based camera, heat-sensitive camera or depth-filtering imaging to limit the active pixel numbers in an image[44–46]. Therefore, our approach provides great hope for the development of high-resolution visual restoration at the cortical level, through its unique combination of a rapid response, high spatial resolution and cell selectivity with promoters. Even if this approach requires craniotomy, as for other existing visual prostheses, it provides a less invasive approach based on deep and distant cortical activation from above the dura mater following AAV cortical injections. More generally, it paves the way for a new type of genetic-based BMI capable of compensating for disabilities and suitable for use in treatments of neurological disorders.

Online content

Any methods, additional references, Nature Portfolio reporting summaries, source data, extended data, supplementary information, acknowledgements, peer review information; details of author contributions and competing interests; and statements of data and code availability are available at https://doi.org/10.1038/s41565-023-01359-6.

References

1. Lebedev, M. A. & Nicolelis, M. A. Brain-machine interfaces: from basic science to neuroprostheses and neurorehabilitation. *Physiol. Rev.* **97**, 767–837 (2017).
2. Lewis, P. M., Ackland, H. M., Lowery, A. J. & Rosenfeld, J. V. Restoration of vision in blind individuals using bionic devices: a review with a focus on cortical visual prostheses. *Brain Res.* **1595**, 51–73 (2015).
3. VanRullen, R. Perceptual cycles. *Trends Cogn. Sci.* **20**, 723–735 (2016).
4. Fernandez, E. et al. Visual percepts evoked with an intracortical 96-channel microelectrode array inserted in human occipital cortex. *J. Clin. Invest.* **131**, e151331 (2021).
5. Beauchamp, M. S. et al. Dynamic stimulation of visual cortex produces form vision in sighted and blind humans. *Cell* **181**, 774–783.e5 (2020).
6. Sahel, J. A. et al. Partial recovery of visual function in a blind patient after optogenetic therapy. *Nat. Med.* **27**, 1223–1229 (2021).
7. Jazayeri, M., Lindbloom-Brown, Z. & Horwitz, G. D. Saccadic eye movements evoked by optogenetic activation of primate V1. *Nat. Neurosci.* **15**, 1368–1370 (2012).
8. Ju, N., Jiang, R., Macknik, S. L., Martinez-Conde, S. & Tang, S. Long-term all-optical interrogation of cortical neurons in awake-behaving nonhuman primates. *PLoS Biol.* **16**, e2005839 (2018).
9. Chernov, M. M., Friedman, R. M., Chen, G., Stoner, G. R. & Roe, A. W. Functionally specific optogenetic modulation in primate visual cortex. *Proc. Natl Acad. Sci. USA* **115**, 10505–10510 (2018).
10. McAlinden, N. et al. Multisite microLED optrode array for neural interfacing. *Neurophoton.* **6**, 035010 (2019).
11. Legon, W. et al. Transcranial focused ultrasound modulates the activity of primary somatosensory cortex in humans. *Nat. Neurosci.* **17**, 322–329 (2014).
12. Tufail, Y. et al. Transcranial pulsed ultrasound stimulates intact brain circuits. *Neuron* **66**, 681–694 (2010).
13. Deffieux, T. et al. Low-intensity focused ultrasound modulates monkey visuomotor behavior. *Curr. Biol.* **23**, 2430–2433 (2013).
14. Lee, W. et al. Image-guided focused ultrasound-mediated regional brain stimulation in sheep. *Ultrasound Med. Biol.* **42**, 459–470 (2016).
15. Tufail, Y., Yoshihiro, A., Pati, S., Li, M. M. & Tyler, W. J. Ultrasonic neuromodulation by brain stimulation with transcranial ultrasound. *Nat. Protoc.* **6**, 1453–1470 (2011).
16. Legon, W., Bansal, P., Tyshynsky, R., Ai, L. & Mueller, J. K. Transcranial focused ultrasound neuromodulation of the human primary motor cortex. *Sci. Rep.* **8**, 10007 (2018).
17. Mehic, E. et al. Increased anatomical specificity of neuromodulation via modulated focused ultrasound. *PLoS ONE* **9**, e86939 (2014).
18. Kim, S. et al. Transcranial focused ultrasound stimulation with high spatial resolution. *Brain Stimul.* **14**, 290–300 (2021).
19. Cheng, Z. et al. High resolution ultrasonic neural modulation observed via in vivo two-photon calcium imaging. *Brain Stimul.* **15**, 190–196 (2022).
20. Ye, P. P., Brown, J. R. & Pauly, K. B. Frequency dependence of ultrasound neurostimulation in the mouse brain. *Ultrasound Med. Biol.* **42**, 1512–1530 (2016).
21. Constans, C., Mateo, P., Tanter, M. & Aubry, J. F. Potential impact of thermal effects during ultrasonic neurostimulation: retrospective numerical estimation of temperature elevation in seven rodent setups. *Phys. Med. Biol.* **63**, 025003 (2018).
22. Yang, Y. et al. Sonogenetics for noninvasive and cellular-level neuromodulation in rodent brain. Preprint at *bioRxiv* https://www.biorxiv.org/content/10.1101/2020.01.28.919910v1 (2020).
23. Qiu, Z. et al. Targeted neurostimulation in mouse brains with non-invasive ultrasound. *Cell Rep.* **32**, 108033 (2020).
24. Huang, Y. S. et al. Sonogenetic modulation of cellular activities using an engineered auditory-sensing protein. *Nano Lett.* **20**, 1089–1100 (2020).
25. Wu, X. et al. Sono-optogenetics facilitated by a circulation-delivered rechargeable light source for minimally invasive optogenetics. *Proc. Natl Acad. Sci. USA* **116**, 26332–26342 (2019).
26. Yang, Y. et al. Sonothermogenetics for noninvasive and cell-type specific deep brain neuromodulation. *Brain Stimul.* **14**, 790–800 (2021).
27. Ye, J. et al. Ultrasonic control of neural activity through activation of the mechanosensitive channel MscL. *Nano Lett.* **18**, 4148–4155 (2018).
28. Soloperto, A. et al. Mechano-sensitization of mammalian neuronal networks through expression of the bacterial large-conductance mechanosensitive ion channel. *J. Cell Sci.* **131**, jcs210393 (2018).
29. Sukharev, S. I., Blount, P., Martinac, B., Blattner, F. R. & Kung, C. A large-conductance mechanosensitive channel in *E. coli* encoded by *mscL* alone. *Nature* **368**, 265–268 (1994).
30. Dalkara, D. et al. In vivo-directed evolution of a new adeno-associated virus for therapeutic outer retinal gene delivery from the vitreous. *Sci. Transl. Med.* **5**, 189ra176 (2013).

31. Chaffiol, A. et al. A new promoter allows optogenetic vision restoration with enhanced sensitivity in macaque retina. *Mol. Ther.* **25**, 2546–2560 (2017).
32. Daich Varela, M., Cabral de Guimaraes, T. A., Georgiou, M. & Michaelides, M. Leber congenital amaurosis/early-onset severe retinal dystrophy: current management and clinical trials. *Br. J. Ophthalmol.* **106**, 445–451 (2022).
33. Verschueren, A. et al. Planar polarity in primate cone photoreceptors: a potential role in Stiles Crawford effect phototropism. *Commun. Biol.* **5**, 89 (2022).
34. Sato, T., Shapiro, M. G. & Tsao, D. Y. Ultrasonic neuromodulation causes widespread cortical activation via an indirect auditory mechanism. *Neuron* **98**, 1031–1041e5 (2018).
35. Guo, H. et al. Ultrasound produces extensive brain activation via a cochlear pathway. *Neuron* **98**, 1020–1030 (2018).
36. Nelidova, D. et al. Restoring light sensitivity using tunable near-infrared sensors. *Science* **368**, 1108–1113 (2020).
37. ter Haar, G. Ultrasound bioeffects and safety. *Proc. Inst. Mech. Eng. H* **224**, 363–373 (2010).
38. Sapareto, S. A. & Dewey, W. C. Thermal dose determination in cancer therapy. *Int. J. Radiat. Oncol. Biol. Phys.* **10**, 787–800 (1984).
39. Aravanis, A. M. et al. An optical neural interface: in vivo control of rodent motor cortex with integrated fiberoptic and optogenetic technology. *J. Neural Eng.* **4**, S143–S156 (2007).
40. Klapoetke, N. C. et al. Independent optical excitation of distinct neural populations. *Nat. Methods* **11**, 338–346 (2014).
41. Chen, R. et al. Deep brain optogenetics without intracranial surgery. *Nat. Biotechnol.* **39**, 161–164 (2021).
42. Flores, A. R. et al. Safety, feasibility, and patient-rated outcome of sonolucent cranioplasty in extracranial-intracranial bypass surgery to allow for transcranioplasty ultrasound assessment. *World Neurosurg.* **144**, e277–e284 (2020).
43. Greenberg, K. P., Pham, A. & Werblin, F. S. Differential targeting of optical neuromodulators to ganglion cell soma and dendrites allows dynamic control of center-surround antagonism. *Neuron* **69**, 713–720 (2011).
44. Lorach, H. et al. Artificial retina: the multichannel processing of the mammalian retina achieved with a neuromorphic asynchronous light acquisition device. *J. Neural Eng.* **9**, 066004 (2012).
45. Kartha, A. et al. Prosthetic visual performance using a disparity-based distance-filtering system. *Transl. Vis. Sci. Technol.* **9**, 27 (2020).
46. Montezuma, S. R. et al. Improved localisation and discrimination of heat emitting household objects with the artificial vision therapy system by integration with thermal sensor. *Br. J. Ophthalmol.* **104**, 1730–1734 (2020).

Methods

Animals

Experiments were conducted in accordance with the National Institutes of Health Guide for the Care and Use of Laboratory Animals. Protocols were approved by the Local Animal Ethics Committee (Committee Charles Darwin no. 5, registration nos. 9529 and 26889) and conducted in agreement with Directive 2010/63/EU of the European Parliament. Long–Evans male rats aged between 2 and 12 months and WT male mice (C57BL/6J) aged 9 weeks were obtained from Janvier Laboratories; P23H (line 1) male transgenic rats (9–22 months) were raised locally.

Plasmid cloning and AAV production

Plasmids containing the *E. coli mscL* sequence in the WT form and with the G22S mutation were obtained from Francesco Difato (Addgene plasmids #107454 and #107455)[28]. To target RGCs, the SNCG promoter[31] was inserted into an AAV backbone plasmid containing the *mscL* sequence fused to the tdTomato gene and the Kir2.1 ER export signal, to drive expression at the plasma membrane. An AAV2.7m8 vector was used for intravitreous delivery. For targeting neurons in the V1 cortical layers, the SNCG promoter was replaced by the CamKII promoter and an AAV9.7m8 vector was chosen. Recombinant AAVs were produced by the plasmid co-transfection method, and the resulting lysates were purified by iodixanol purification[31].

US stimulus

Three focused US transducers with different central frequencies were used: 0.50 MHz (diameter, $Ø = 1.00'' = 25.4$ mm; focal distance, $f = 1.25'' = 31.7$ mm) (V301-SU, Olympus), 2.25 MHz ($Ø = 0.50'' = 12.7$ mm, $f = 1.00'' = 25.4$ mm) (V306-SU, Olympus) and 15.00 MHz ($Ø = 0.50'' = 12.7$ mm, $f = 1.00'' = 25.4$ mm) (V319-SU, Olympus), corresponding to numerical apertures of $F/Ø = 1.25$ and 2.00. Acoustic fields radiated by those three focused transducers are presented in Fig. 1 (simulations) and Extended Data Fig. 3 (experimental measurements). A TiePie Handyscope (HS5, TiePie Engineering) was used to produce the stimulus waveform, which was then passed through an 80 dB RF power amplifier (VBA 230-80, Vectawave) connected to the transducer. Transducer pressure outputs (pressure at focus, three-dimensional (3D) pressure maps) were measured in a degassed water tank with a Royer–Dieulesaint heterodyne interferometer[47]. US stimuli used for ex vivo and in vivo stimulation had the following characteristics: 1 kHz pulse repetition frequency with a 50% duty cycle, sonication duration between 10 and 200 ms and interstimulus interval between 0.01 and 2.00 s. Peak acoustic pressures ranged from 0.11 to 0.88 MPa, 0.30 to 1.60 MPa and 0.20 to 1.27 MPa for the 0.50, 2.25 and 15.00 MHz transducers, respectively. The corresponding estimated spatial peak pulse average intensity (Isppa) values were 0.39–25.14, 2.92–83.12 and 1.30–52.37 W cm^{-2}.

Intravitreous gene delivery and retinal imaging

Rats were anaesthetized[48] and AAV suspension (2 µl), containing between 8 and 14×10^{10} viral particles, was injected into the centre of the vitreous cavity. One month later, tdTomato fluorescence imaging was performed on the injected eyes, with a MICRON IV retinal imaging microscope (Phoenix Research Laboratories) and Micron Discover v.2.2.

MEA recordings

Retinal pieces were flattened on a filter membrane (Whatman, GE Healthcare Life Sciences) and placed on an MEA (electrode diameter, 30 µm; spacing, 200 µm; MEA256 200/30 iR-ITO, MultiChannel Systems) coated with poly-L-lysine (0.1%, Sigma), with RGCs facing the electrodes[31]. AMPA/kainate glutamate receptor antagonist 6-cyano-7-nitroquinoxaline-2,3-dione (CNQX, 25 µM, Sigma-Aldrich), the NMDA glutamate receptor antagonist [3H]3-(2-carboxypiperazin-4-yl) propyl-1-phosphonic acid (CPP, 10 µM, Sigma-Aldrich) and a selective group III metabotropic glutamate receptor agonist, L-(+)-2-amino-4-phosphonobutyric acid (LAP4, 50 µM, Tocris Bioscience), were bath applied through the perfusion line. Light stimuli were delivered with a digital micromirror display (Vialux; resolution, 1,024 × 768) coupled to a white light-emitting diode light source (MNWHL4, Thorlabs) focused on the photoreceptor plane (irradiance, 1 µW cm^{-2}). US transducers were coupled with a custom-made coupling cone filled with degassed water and mounted on a motorized stage (PT3/M-Z8, Thorlabs) placed orthogonally above the retina. The reflected signal of the MEA chip and the retina was detected with a US key device (Lecoeur Electronique). The distance between the retina and transducer was equal to the focal length of the transducer; this was verified with the flight time of the reflected signal. From RGC recordings with a 252 channel preamplifier and MC_Rack v. 4.6.2 (MultiChannel Systems), spikes were sorted with Spyking CIRCUS 0.5 software[49]. RGC responses were analysed with custom scripts written in MATLAB (MathWorks 2018b) for classification as ON, ON–OFF or OFF, with the response dominance index[50]. Latencies were calculated as the time between stimulus onset and the maximum of the derivative of the spike density function (SDF). Two classes of US-responding cells were identified on the basis of latency—SL and LL—by fixing a threshold equal to the minimum of the latency distribution of the responses of NT cells to US (45 ms). We determined the peak value A of the SDF for the calculation of response duration, which was defined as the time interval between the two time points for which the SDF was equal to A/e (where A is peak depolarization and e is Euler's number). The Fano factor, quantifying spike count variability, was calculated as the ratio of the variance of the spike count to the mean. The Euclidean distance between two activated cells was weighted according to the maximum firing rate of the cells. The ratio of the number of activated cells to the size of the area stimulated on the MEA chip was calculated considering the size of the US focal spot for 2.25 and 15.00 MHz and the size of the MEA for 0.50 MHz, because the focal spot was larger than the MEA for this frequency. The centre of the response was estimated by weighting the maximum firing rate of each cell by its distance from other responding cells, and the displacement of the response was calculated as the Euclidean distance between two centre-of-response positions.

Intracranial injections

AAV suspensions were injected into the right hemisphere at two different locations in rats (2.6 mm ML, 6.8 mm AP and 3.1 mm ML, 7.2 mm AP from the bregma) or at one location in mice (2.5 mm ML, 3.5 mm AP from the bregma)[48]. For rat injections, the suspension (200 nl containing $0.2–8.0 \times 10^{15}$ viral particles) was injected at three different depths (1,100, 1,350 and 1,500 µm from the cortical surface) with a microsyringe pump controller (Micro4, World Precision Instruments) operating at a rate of 50 nl min^{-1} and 10 µl Hamilton syringe. In mice, the AAV suspension (1 µl containing $0.2–8.0 \times 10^{15}$ viral particles) was injected at 400 µm from the cortical surface at a rate of 100 nl min^{-1}.

In vivo extracellular recordings

One month after AAV injections, a small craniotomy (5 × 5 mm^2) was performed above V1 in the right hemisphere[48]. The tdTomato fluorescence was checked with a MICRON IV retinal imaging microscope and Micron Discover v. 2.2 (Phoenix Research Laboratories). A 32 site µEcog electrode array (electrode diameter, 30 µm; electrode spacing, 300 µm; FlexMEA36, MultiChannel Systems) was positioned over the transfected region or in a similar zone for control rats. MEA recordings were performed with a 16 site silicon microprobe tilted at 45° to the brain surface (electrode diameter, 30 µm; spacing, 50 µm; A1x16-5mm-50-703, NeuroNexus Technologies) and MC_Rack v. 4.6.2. The MEA was advanced 1,100 µm into the cortex with a three-axis micromanipulator (Sutter Instruments). US transducers were coupled to the brain with a custom-made coupling cone filled with degassed water and US gel on a motorized stage. The distance between the cortex and

transducer was equal to the focal length of the transducer. Visual stimuli were generated by a white-light-collimated light-emitting diode (MNWHL4, Thorlabs) placed 15 cm away from the eye (4.5 mW cm^{-2} at the cornea). Recordings were digitized with 32 channel and 16 channel amplifiers (model ME32/16-FAI-µPA, MultiChannel Systems). The µEcog recordings were analysed with custom-developed MATLAB scripts and the MEA recordings were analysed with Spyking CIRCUS software and custom-developed MATLAB scripts. The response duration was calculated as the interval between the two time points at which the cortical-evoked potential was equal to A/e. The activated area was defined as the area of the pseudocolour activation map over which peak depolarization exceeded the background-noise level calculated as 2 × s.d. of the signal. The response centre was estimated by weighting the peak depolarization of each electrode by its distance from the other electrodes. Its relative displacement when moving the US transducer was calculated as the Euclidean distance of the two positions. For intracortical recordings, cell latency was estimated as the time between stimulus onset and the maximum of the derivative of SDF.

Surgery for in vivo behavioural testing

C57BL6J mice were subcutaneously injected with buprenorphine (0.05 mg kg^{-1}) (Buprécare, Axience), and dexamethasone (0.7 mg kg^{-1}) (Dexazone, Virbac). Animals were anaesthetized with isoflurane (5% induction and 2% maintenance, in an air/oxygen mixture) and the head was shaved and cleaned with an antiseptic solution. Animals were head fixed on a stereotactic frame with an isoflurane delivery system and eye ointment, and a black tissue was applied over the eyes. The body temperature was maintained at 37 °C. After a local injection of lidocaïne (4 mg kg^{-1}) (Laocaïne, Centravet), an incision was made on the skin. Two screws were fixed in the skull, after a small craniotomy (approximately 5.0 × 5.0 mm^2) was performed above V1 in the right hemisphere (0.5 mm steel drill) and a cortex buffer was applied. The cortex was covered with a TPX plastic sheet (125 µm thick) and sealed with dental acrylic cement (Tetric Evoflow). For behavioural experiments, a metallic headbar (PhenoSys) for head fixation was then glued to the skull on the left hemisphere with dental cement (FujiCEM 2). Animals were placed in a recovery chamber, with a subcutaneous injection of physiological serum and ointment on the eyes (Ophtalon, Centravet). Buprenorphine was injected during post-surgery monitoring.

Mouse behavioural tests

Mice were placed on a water restriction schedule until they reached approximately 80–85% of their weight. Following habituation to the test conditions[36], mice were trained to respond to an LS by performing a voluntary detection task: licking a waterspout (blunt 18 gauge needle, approximately 5 mm from the mouth) in response to white-light full-field stimulation (200 and 50 ms long) of the left eye (dilated with tropicamide, Mydriaticum Dispersa) over 35 trials per stimulation duration and therefore 70 trials per day. Water (~4 µl) was automatically dispensed 500 ms after the light was switched on, through a calibrated water system. The behavioural protocol and lick detection were controlled by a custom-made system[36]. The next four days (two-day break during the weekend), US stimulations were delivered on V1 for 50 ms at three different pressure values (0.2, 0.7 and 1.2 MPa). These pressure values were delivered in a different order each day (35 trials each). The intertrial intervals randomly varied and ranged between 10 and 30 s. The 15 MHz US transducer was coupled to the brain with a custom-made coupling cone filled with water and US gel. The success rate was calculated by counting the number of trials in which the mice performed anticipatory licks (between stimulus onset and the opening of the water valve). The anticipatory lick rate (Fig. 6e) for the session was calculated by subtraction from the anticipatory lick rate of a trial, the spontaneous lick rate (calculated on all the 1 s time windows before each individual stimulus onset (Fig. 6a) for all the trials) and multiplication by the success rate. Lick latency was calculated by determining the time to the first anticipatory lick after stimulus onset. The mice retained for analysis presented a success rate superior or equal to 60% on the fourth day following LS. Then, light or US sessions showing a compulsive licking behaviour were excluded based on the outlier identification made using the ROUT method (Q = 1%) on the session's spontaneous lick rate averaging the measurements on all the trials of the session in the 1 s time window before the stimulus onset of the trial.

Immunohistochemistry and confocal imaging

Samples were incubated overnight at 4 °C with a monoclonal anti-RBPMS antibody (1:500, rabbit; ABN1362, Merck Millipore) for the retina[31], with a monoclonal anti-NeuN antibody (1:500, mouse, clone A60; MAB377, Merck Millipore) for brain sections[48]. The sections were then incubated with secondary antibodies conjugated with Alexa Fluor 488 (1:500, donkey anti-mouse and donkey anti-rabbit IgG 488, polyclonal; A-21202 and A-21206, Invitrogen, respectively) and DAPI (1:1,000; D9542, Merck Millipore) for 1 h at room temperature. An Olympus FV1000 confocal microscope with ×20 objective (UPLSAPO 20XO with a numerical aperture of 0.85) was used to acquire the images of flat-mounted retinas and brain sections (FV10-ASW v. 4.2 software).

On the confocal images processed with Fiji (ImageJ v. 1.53q), RBPMS- and NeuN-positive cells were automatically counted with the 'analyze particles' plugin. The cells were manually counted by two different users, with the 'cell counter' plugin. Quantification was performed by acquiring confocal stacks in at least four randomly chosen transfected regions of 0.4 mm^2 (Extended Data Fig. 1). For V1 neurons, the sagittal brain slice with the largest tdTomato fluorescence zone was selected for each animal. A region of interest was manually defined in V1 and the quantifications were performed in at least six randomly chosen regions of 0.4 mm^2.

US-induced tissue-heating simulations

A three-fold process was used for the estimation of thermal effects: (1) simulation of the acoustic fields generated by the three transducers, with realistic acoustic parameters; (2) verification that nonlinear acoustics did not play an important role in heat transfer; and (3) realistic simulations of heat transfer and temperature rise induced at the focus by US in a linear regime for the parameters used in this study.

For nonlinear simulations, we used MATLAB's k-Wave toolbox by defining the geometry of the transducer in three dimensions and using the following parameters for the propagation medium (water): sound speed, c = 1,500 m s^{-1}; volumetric mass, ρ = 1,000 kg m^{-3}; nonlinearity coefficient, B/A = 5; attenuation coefficient, $\alpha = 2.2 \times 10^{-3}$ dB cm^{-1} MHz^{-y}; frequency power law of the attenuation coefficient, y = 2 (ref. 51). We simulated quasi-monochromatic 3D wavefields using long bursts of 50 cycles; this gave us the maximum pressure field in three dimensions as well as the waveform at the focus. Simulations were calibrated by adjusting the input pressure (excitation of the simulated transducer) to reach the pressure at the focus measured in the water tank with real transducers. The full-width at half-maximum (FWHM) focal-spot diameter in the x–y plane was 4.360, 1.610 and 0.276 mm, and the length of the major axis in the x–z plane was 32.3, 20.6 and 3.75 mm for the 0.50, 2.25 and 15.00 MHz transducers, respectively (Fig. 1b–d). Nonlinear effects were evaluated by estimating the relative harmonic content of the waveform at the focus. In the 15 MHz focus transducer example in Fig. 1d, the experimental and simulated signals at the focal spot were compared and found to be highly concordant (Extended Data Fig. 4a). Furthermore, the amplitude of the second harmonic is 19.8 dB below the fundamental (20.9 dB in the simulated case), meaning that if the fundamental energy is E, the second harmonic has energy E/95 (Extended Data Fig. 4b). Therefore, we can reasonably neglect the nonlinear effects in the calculations of the thermal effects,

as they account for ~1% of the energy involved. The same conclusions were drawn at 0.5 MHz and 15.0 MHz. Linear wave propagation approximations considerably decreased the computing cost of the simulations. Linear propagation simulations were conducted with the Field II toolbox in MATLAB[52,53], in the monochromatic mode, with the same medium properties as k-Wave (water), to obtain the 3D maximum pressure fields. These maximum pressure fields were used to build a heating source term $Q_{US} = \frac{\alpha_{np} p_{max}^2}{\rho_b c_b}$, where α_{np} is the absorption coefficient of the brain at the considered frequency (59.04 Np m^{-1} at 15 MHz, calculated from $\alpha_{brain} = 0.21$ dB cm^{-1} MHz^{-y} and $y = 1.18$), the brain volumetric mass $\rho_{brain} = 1{,}046$ kg m^{-3}, the brain sound speed $c_{brain} = 154$ s^{-1} and p_{max} is the 3D maximum pressure field. This source term was then used in the resolution of a Penne's bioheat equation $\rho_{brain} C_{brain} \times \frac{\partial T}{\partial t} = \mathrm{div}\,(K_t \times \nabla T) - \rho_{blood} C_{blood} P_{blood}\,(T - T_a) + Q$ in k-Wave, where C_{brain} is the blood specific heat capacity (3,630 J kg^{-1} °C^{-1}), K_t is the brain thermal conductivity (0.51 W m^{-1} °C^{-1}), ρ_{blood} is the blood density (1,050 kg m^{-3}), C_{blood} is the blood specific heat capacity (3,617 J kg^{-1} °C^{-1}), P_{blood} is the blood perfusion coefficient (9.7×10^{-3} s^{-1}), T_a is the arterial temperature (37 °C), $Q = Q_{US} + \rho_{brain} \gamma_{brain}$ and γ_{brain} is the heat generation of the brain tissue (11.37 W kg^{-1}) (refs. 54,55). The initial condition for brain temperature was set to $T_0 = 37$ °C.

This simulation corresponds to the worst-case scenario regarding the given temperature rise. (1) The acoustic propagation is simulated in water only (non-derated value), with a lower attenuation coefficient (2.2×10^{-3} dB cm MHz$^{-2.00}$) than the brain (0.59 dB cm MHz$^{-1.27}$), even if a part of the propagation occurs within the brain. The p_{max} maps are, therefore, overestimated. (2) Thermal absorption is simulated in the brain tissue only, with a higher absorption coefficient (0.21 dB cm MHz$^{-1.18}$) than water, even if a part of the maximum pressure field is actually located within the water of the acoustic coupling cone. Therefore, Q_{US} is slightly overestimated. We mapped the temperature in three spatial dimensions and time, and looked for the point of maximum temperature rise (Extended Data Fig. 4c–f).

Statistical analysis

Statistical analyses were carried out with Prism software (Prism 9, GraphPad). Values are expressed and represented as mean values ± standard error of the mean (s.e.m.) on figures and in the text, unless specified otherwise. Data were analysed in unpaired Welch's *t*-tests (two tailed) or an unpaired multiple *t*-test with Sidak–Bonferroni correction for multiple comparisons. Statistical tests are provided in the figure legends.

Reporting summary

Further information on research design is available in the Nature Portfolio Reporting Summary linked to this article.

Data availability

Data supporting the findings of this study are available within the Article and via FigShare at https://figshare.com/projects/Ectopic_expression_of_a_mechanosensitive_channel_confers_spatiotemporal_resolution_to_ultrasound_stimulations_of_neuronal_circuits_for_visual_restoration/154041. All other data are available from the corresponding author upon reasonable request. Source data are provided with this paper.

Code availability

The custom MATLAB codes are available from the corresponding author upon request.

References

47. Royer, D. & Dieulesaint, E. Optical probing of the mechanical impulse response of a transducer. *Appl. Phys. Lett.* **49**, 1056–1058 (1986).
48. Provansal, M. et al. Functional ultrasound imaging of the spreading activity following optogenetic stimulation of the rat visual cortex. *Sci. Rep.* **11**, 12603 (2021).
49. Yger, P. et al. A spike sorting toolbox for up to thousands of electrodes validated with ground truth recordings in vitro and in vivo. *eLife* **7**, e34518 (2018).
50. Akerman, C. J., Smyth, D. & Thompson, I. D. Visual experience before eye-opening and the development of the retinogeniculate pathway. *Neuron* **36**, 869–879 (2002).
51. Duck, F. A. *Physical Properties of Tissues: A Comprehensive Reference Network* (Academic Press, 2013).
52. Jensen, J. A. & Svendsen, N. B. Calculation of pressure fields from arbitrarily shaped, apodized, and excited ultrasound transducers. *IEEE Trans. Ultrason., Ferroelectr., Freq. Control* **39**, 262–267 (1992).
53. Jensen, J. A. A program for simulating ultrasound systems. *Med. Biol. Eng. Comput.* **34**, 351–353 (1996).
54. Hasgall, P. A. et al. *IT'IS Database for Thermal and Electromagnetic Parameters of Biological Tissues* (accessed 17 August 2020); https://itis.swiss/virtual-population/tissue-properties/
55. McIntosh, R. L. & Anderson, V. A. A comprehensive tissue properties database provided for the thermal assessment of a human at rest. *Biophys. Rev. Lett.* **5**, 129–151 (2010).

Acknowledgements

We would like to thank C. Joffrois, M. Valet, Q. Cesar, M. Desrosiers, S. Fouquet, P. Annic, M. Celik and Z. Raics for technical help and scientific advice. This work was supported by the European Research Council (ERC) Synergy Grant Scheme (holistic evaluation of light and multiwave applications to high-resolution imaging in ophthalmic translational research revisiting the Helmholtzian synergies, ERC grant agreement no. 610110), by the European Union's Horizon 2020 research and innovation programme under grant agreement no. 785219 (Graphene Flagship Core 2) and no. 881603 (Graphene Flagship Core 3); by the Foundation Fighting Blindness; La Fondation pour la Recherche Médicale (FRM EQUIPE EQU202106012159); L'UNIM; la Fédération des Aveugles de France; Optic 2000; the city of Paris; Région ile de France; the Agence Nationale de la Recherche (ANR BrainOptoSight); and French state funds managed by the Agence Nationale de la Recherche (ANR) within Programme Investissements d'Avenir, Laboratoire d'Excellence (LABEX) LIFESENSES (ANR-10-LABX-0065) and Institut Hospitalo-Universitaire FOReSIGHT (ANR-18-IAHU-0001); by NIH CORE Grant P30 EY08098 to the Department of Ophthalmology, the Eye and Ear Foundation of Pittsburgh; and from an unrestricted grant from Research to Prevent Blindness, New York.

Author contributions

S.C. and C.D. designed the experiments. S.C., M.P., G.L., I.A., J.L, R.G., E.B. and J.D. carried out the experiments and analysed the data. M.P., D.Ng., D. Ne., G.G., F.A., O.M., D.D., M.S. and B.R. provided support for the experiments, study design and data analysis. S.P., M.T. and J.S. conceived the idea for this project and supervised the analysis of the obtained data. S.C., C.D, I.A., M.T. and S.P. wrote the manuscript. All the authors provided critical feedback on the research and the manuscript.

Competing interests

The authors have filed for a patent in Europe (PCT/EP2021/074868) for devices and methods for sonogenetic stimulation.

Additional information

Extended data is available for this paper at https://doi.org/10.1038/s41565-023-01359-6.

Supplementary information The online version contains supplementary material available at https://doi.org/10.1038/s41565-023-01359-6.

Correspondence and requests for materials should be addressed to Serge Picaud.

Peer review information *Nature Nanotechnology* thanks Pengfei Song and the other, anonymous, reviewer(s) for their contribution to the peer review of this work.

https://doi.org/10.1038/s41565-023-01359-6

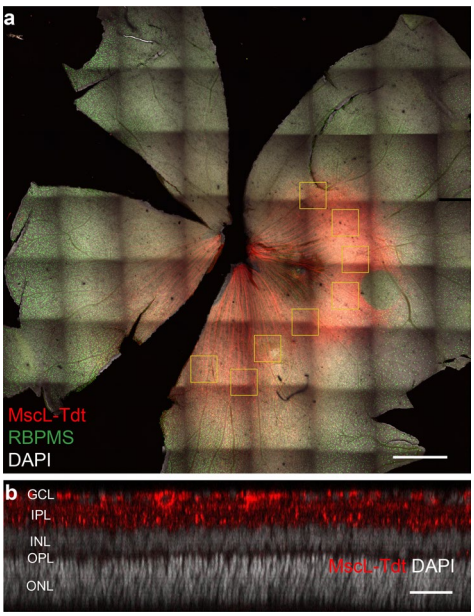

Extended Data Fig. 1 | Retinal expression of MscL. (a) Whole-mount retina expressing MscL WT (red) and labeled with the RGC-specific anti-RBPMS antibody (green), with DAPI staining of the nucleus (white). Yellow boxes represent the 8 zones selected for the counting of MscL- and RBPMS-positive cells. (b) Optical section of a confocal stack showing MscL expression limited to the ganglion cell layer. The scale bars represent 1 mm in (a), 50 µm in (b). Similar results have been obtained for N = 10 retinas (5 expressing MscL WT and 5 expressing MscL G22s).

https://doi.org/10.1038/s41565-023-01359-6

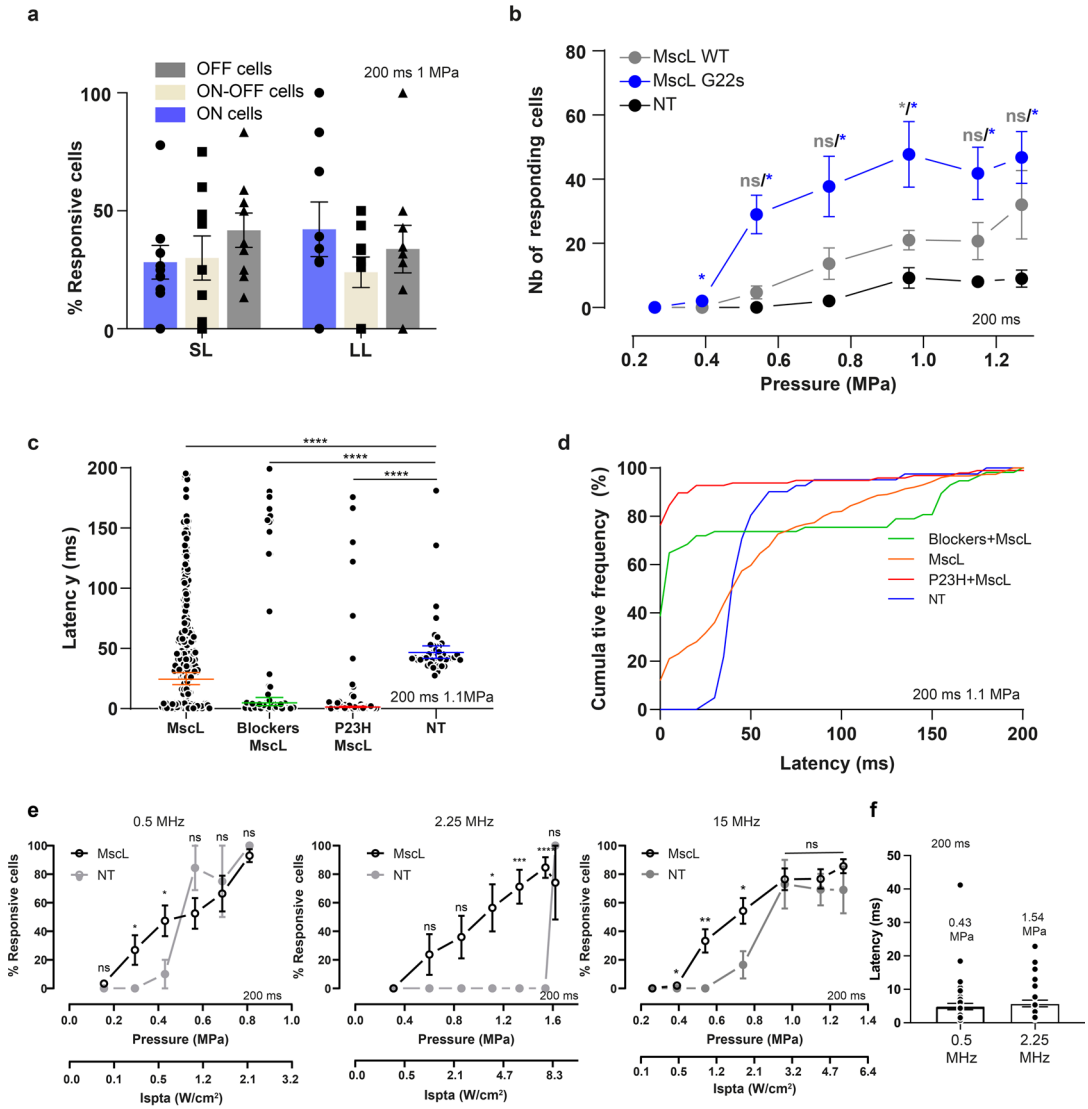

Extended Data Fig. 2 | Retinal sonogenetic response characteristics for US stimuli of different frequencies. (a) Mean distributions of the different RGC cell types (ON, OFF, ON-OFF) among short (SL) and long latency (LL) responses in retinas ($n = 9$) expressing MscL (WT and G22s form) following a 15 MHz US stimulus (SD: 21.6, 28.0, 21.8 % for SL, 34.7, 19.4, 30.3 % for LL cells, for ON, ON-OFF and OFF cells respectively). (b) Mean numbers of RGCs responding to a 15 MHz stimulus of increasing acoustic pressure for MscL WT ($n = 3$), MscL G22s ($n = 5$) and NT ($n = 4$) retinas (0.39 MPa: * $p = 0.0163$; 0.54 MPa: ns $p = 0.1480$, * $p = 0.0168$; 0.74 MPa: ns $p = 0.1334$, * $p = 0.0312$; 0.96 MPa: * $p = 0.0462$, * $p = 0.0279$; 1.15 MPa: ns $p = 0.1617$, * $p = 0.0145$; 1.27 MPa: ns $p = 0.1580$, * $p = 0.0144$; unpaired two-tailed t test between MscL WT and NT in gray and MscL-G22s and NT in blue). (c) Scatter plots and geometric means of RGC latencies in response to a 15 MHz US stimulus for MscL ($n = 300$ cells SD: 48.8), Blockers+MscL ($n = 57$ cells, SD: 68.0), P23H + MscL ($n = 97$ cells, SD: 37.5), and NT ($n = 41$ cells, SD: 27.4) retinas (****, p = $7.3*10^{-8}$ for MscL and Blockers MscL vs NT and $p < .1*10^{-15}$ for P23H MscL vs NT, unpaired two-tailed t-test on log-transformed values). (d) Cumulative frequency distributions of RGC latencies for MscL, Blockers+MscL, P23H + MscL, and NT retinas. (e) Mean percentages of cells responding to US stimuli (normalized against the maximum number of responsive cells in the experiment) of increasing acoustic pressure for 0.5 MHz (ns $p = 0.1661$;* $p = 0.0292$; * $p = 0.0260$; ns $p = 0.8628$; ns $p = 0.1316$; ns $p = 0.7731$; unpaired t test,), 2.25 MHz (ns $p = 0.1474$; ns $p = 0.0522$; * $p = 0.0140$; *** $p = 0.0005$; **** $p < 0.00002$; ns $p = 0.5000$; unpaired t test) and 15 MHz US (* $p = 0.0382$;** $p = 0.0065$; * $p = 0.0218$; ns $p = 0.8628$; ns $p = 0.5859$; ns $p = 0.4223$; unpaired t test) US. The lower x axis represents the corresponding acoustic intensity (Ispta). (f) Mean response latencies of SL cells for 0.5 and 2.25 MHz ($n = 9$ and 8 retinas). Data are presented as mean values + /- SEM.

https://doi.org/10.1038/s41565-023-01359-6

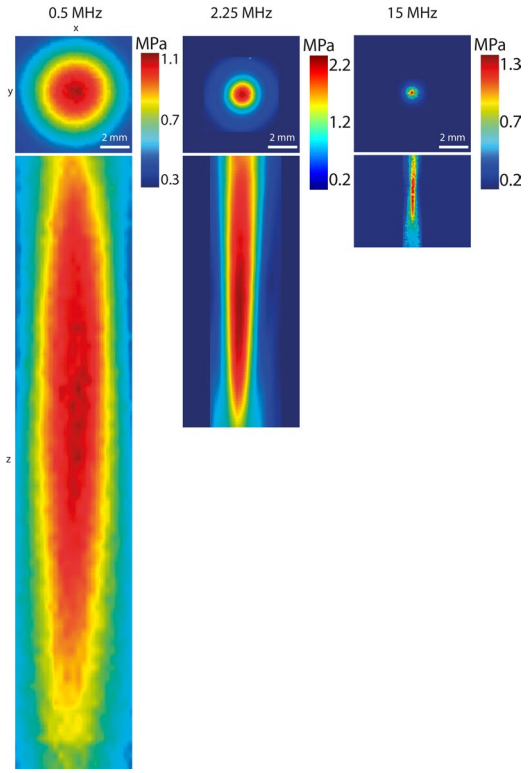

Extended Data Fig. 3 | Experimentally measured US pressure fields. US pressure fields near the focus for 0.5, 2.25 and 15 MHz focused transducers, measured in water. Color-coded pressure maps in the *xy* and *xz* planes, for 0.5, 2.25 and 15 MHz.

https://doi.org/10.1038/s41565-023-01359-6

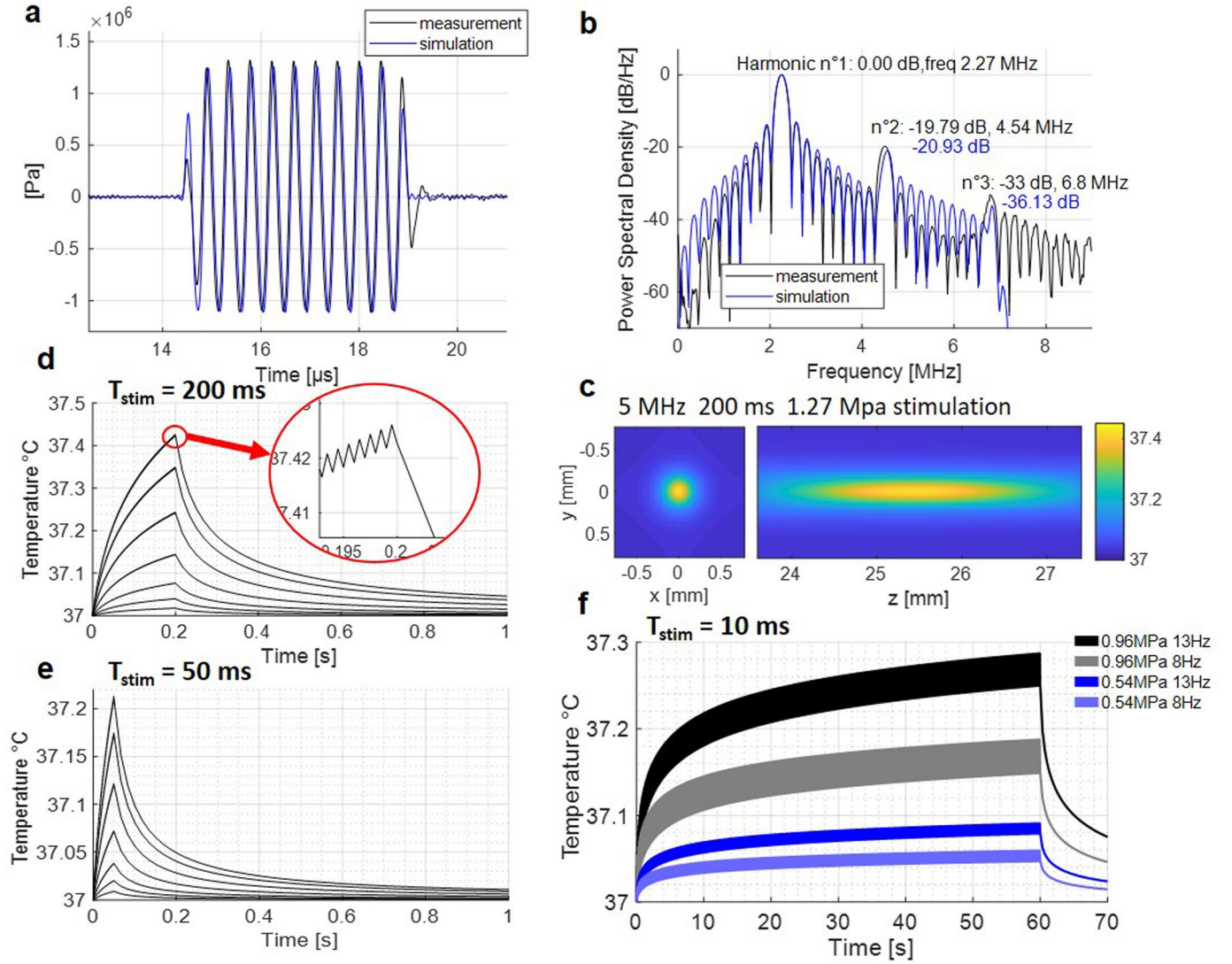

Extended Data Fig. 4 | Simulated acoustic fields and temperature increases. (a) Comparison between a water tank measurement at the focus with a calibrated hydrophone (black) obtained with the 2.25 MHz transducer and reaching -1.11 MPa peak negative pressure, and a simulated waveform at the focus (blue) reaching the same negative pressure. The two waveforms match very well (0.42% error) ensuring a good match between our simulation setup and physical parameters. (b) Power spectral density of the measured (black) and simulated (blue) waveforms, showing that simulations can be used to estimate the importance of non-linear propagation. A second harmonic 20 dB below the fundamental indicates a factor of 100 in terms of energy, meaning that absorption can be calculated in a linear approximation. (c-f) Thermal simulations are performed in a two-fold process corresponding to a worst-case scenario (see methods): propagation in a water medium, and thermal absorption in a brain-mimicking medium. (h) 3D temperature map at the end of a 200 ms stimulation (at 15 MHz and 1.27 MPa). (d) Temperature rise at the focus for a 15 MHz 200 ms stimulation with the 7 pressures used in Fig. 1l (0.26, 0.39, 0.54, 0.74, 0.96, 1.15, 1.27 MPa). A zoom on the increasing curve reveals the fluctuations due to the 1 kHz on-off cycles. (e) Temperature rise at the focus for a 15 MHz 50 ms stimulation with the same 7 pressures. (f) Temperature rise at the focus for 15 MHz 10 ms stimulations (1 kHz modulation) at a repetition rate of 8 Hz and 13 Hz (used in Fig. 3o), for focus pressures of 0.96 MPa and 0.54 MPa.

https://doi.org/10.1038/s41565-023-01359-6

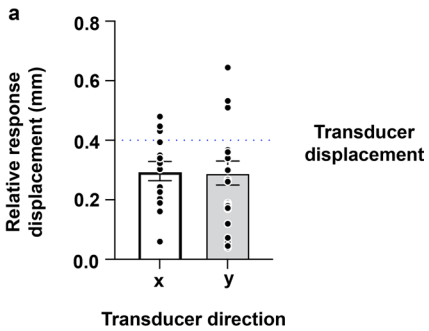

Extended Data Fig. 5 | In vivo response displacement to US stimulation. (a) Relative displacement of the activation center to the previous position following movement of the US transducer by 0.4 mm in the x and y direction (n = 37 positions on 6 animals). Data are presented as mean values + /- SEM.

https://doi.org/10.1038/s41565-023-01359-6

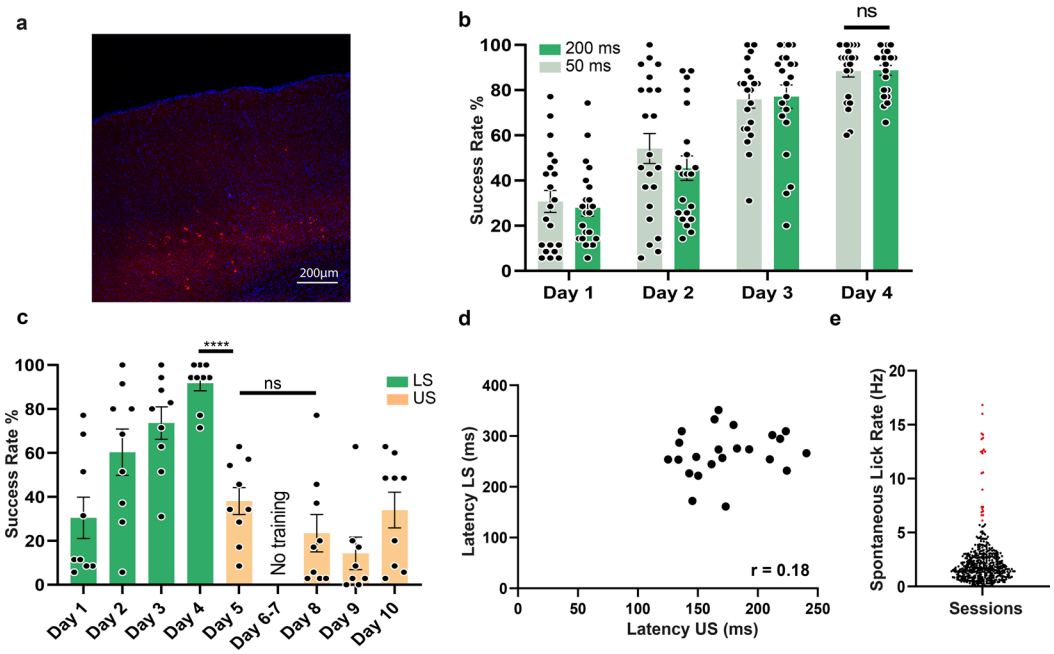

Extended Data Fig. 6 | MscL G22S expression with the US and light-associative training in mice. (a) Confocal stack projection of a sagittal brain slice expressing MscL G22s-tdTomato (red) and labeled with DAPI (blue). Similar results have been obtained on N = 3 animals. (b) Head-fixed and water-restricted mice were trained for four days to respond to a full-field stimulation of one eye (200 and 50 ms) that preceded a water reward. Mice responded by licking before (anticipation – successful trial) or after the delivery of water (failure). The mean success rate increased progressively and mice learned the task (upon 50 ms and 200 ms light stimulation) after four days of training (ns $p = 0.9387$, two-tailed unpaired t test, Mean: 27.9, 45.4, 77.1, 88.8, SD: 17.4, 24.8, 23.6, 10.4% for 200 ms, Mean: 30.7, 54.2, 75.9, 88.5, SD: 22.2, 31.0, 17.5, 12.8% for 50 ms). (c) Mean rates of successful trials in non-transfected (NT) mice for 4 days of training with light stimulation (50 ms, LS green) and for 4 days of US stimulation (US orange) (Between Day 4 LS and Day 5 US: 50 ms 1.2 MPa, ****, $p = 0.0000047$, two-tailed unpaired t test. Between Day 5 US and Day 8 US: 50 ms 1.2 MPa, ns, $p = 0.1850$. Mean: 30.5, 60.3, 73.6, 91.7, 38.1, 23.5, 14.3, 34.0, SD: 28.2, 31.6, 22.1, 10.3, 18.5, 25.5, 21.1, 24.4 %). (d) Pearson correlation scatter plot for time to first lick after either light (LS) or US stimulation. (e) Identification and exclusion of outlier sessions (in red) based on the ROUT method, (Q = 1%) for the session spontaneous lick rate measured on a 1 s time window prior to all trials of the session e $Q_1 = 0.9$ Hz, Median = 1.7 Hz, $Q_3 = 2.8$ Hz, Mean= 2.3 Hz, SD = 2.3 Hz. Data are presented as mean values + /- SEM.

nature portfolio

Corresponding author(s): Serge Picaud

Last updated by author(s): 27/01/223

Reporting Summary

Nature Portfolio wishes to improve the reproducibility of the work that we publish. This form provides structure for consistency and transparency in reporting. For further information on Nature Portfolio policies, see our Editorial Policies and the Editorial Policy Checklist.

Statistics

For all statistical analyses, confirm that the following items are present in the figure legend, table legend, main text, or Methods section.

n/a	Confirmed
☐	☒ The exact sample size (*n*) for each experimental group/condition, given as a discrete number and unit of measurement
☐	☒ A statement on whether measurements were taken from distinct samples or whether the same sample was measured repeatedly
☐	☒ The statistical test(s) used AND whether they are one- or two-sided *Only common tests should be described solely by name; describe more complex techniques in the Methods section.*
☒	☐ A description of all covariates tested
☒	☐ A description of any assumptions or corrections, such as tests of normality and adjustment for multiple comparisons
☐	☒ A full description of the statistical parameters including central tendency (e.g. means) or other basic estimates (e.g. regression coefficient) AND variation (e.g. standard deviation) or associated estimates of uncertainty (e.g. confidence intervals)
☐	☒ For null hypothesis testing, the test statistic (e.g. *F*, *t*, *r*) with confidence intervals, effect sizes, degrees of freedom and *P* value noted *Give P values as exact values whenever suitable.*
☒	☐ For Bayesian analysis, information on the choice of priors and Markov chain Monte Carlo settings
☒	☐ For hierarchical and complex designs, identification of the appropriate level for tests and full reporting of outcomes
☐	☒ Estimates of effect sizes (e.g. Cohen's *d*, Pearson's *r*), indicating how they were calculated

Our web collection on statistics for biologists contains articles on many of the points above.

Software and code

Policy information about availability of computer code

Data collection	MC-rack Multichannel System, Phoenix microm imaging software, olympus fluoview FV100
Data analysis	Multichannel systems data analysis V 2.6.15, Spyking Circus 0;5, Matlab, GraphPad Prism 9, Fiji ImageJ 1.53q

For manuscripts utilizing custom algorithms or software that are central to the research but not yet described in published literature, software must be made available to editors and reviewers. We strongly encourage code deposition in a community repository (e.g. GitHub). See the Nature Portfolio guidelines for submitting code & software for further information.

Data

Policy information about availability of data

All manuscripts must include a data availability statement. This statement should provide the following information, where applicable:

- Accession codes, unique identifiers, or web links for publicly available datasets
- A description of any restrictions on data availability
- For clinical datasets or third party data, please ensure that the statement adheres to our policy

Some dara are already available on fighshare (https://figshare.com/account/home#/projects/154041) and more are available on demand from the corresponding author

Human research participants

Policy information about studies involving human research participants and Sex and Gender in Research.

Reporting on sex and gender	*Use the terms sex (biological attribute) and gender (shaped by social and cultural circumstances) carefully in order to avoid confusing both terms. Indicate if findings apply to only one sex or gender; describe whether sex and gender were considered in study design whether sex and/or gender was determined based on self-reporting or assigned and methods used. Provide in the source data disaggregated sex and gender data where this information has been collected, and consent has been obtained for sharing of individual-level data; provide overall numbers in this Reporting Summary. Please state if this information has not been collected. Report sex- and gender-based analyses where performed, justify reasons for lack of sex- and gender-based analysis.*
Population characteristics	*Describe the covariate-relevant population characteristics of the human research participants (e.g. age, genotypic information, past and current diagnosis and treatment categories). If you filled out the behavioural & social sciences study design questions and have nothing to add here, write "See above."*
Recruitment	*Describe how participants were recruited. Outline any potential self-selection bias or other biases that may be present and how these are likely to impact results.*
Ethics oversight	*Identify the organization(s) that approved the study protocol.*

Note that full information on the approval of the study protocol must also be provided in the manuscript.

Field-specific reporting

Please select the one below that is the best fit for your research. If you are not sure, read the appropriate sections before making your selection.

☒ Life sciences ☐ Behavioural & social sciences ☐ Ecological, evolutionary & environmental sciences

For a reference copy of the document with all sections, see nature.com/documents/nr-reporting-summary-flat.pdf

Life sciences study design

All studies must disclose on these points even when the disclosure is negative.

Sample size	Sample sizes were not predetermined but some were increased based on reviewers' demand. They were defined to obtain statistically significant diffeences (evaluated using two-sided unpaired t-test) between the transfected and non-transfected groups.
Data exclusions	No data were excluded for the analysis.
Replication	To verify reproducibility, each stimulation was repeated at least 50 times for each stimulation on several animals. Replications were successfull for each tested preparation
Randomization	Recordings were performed with random allocation between transfected and non-transfected groups. When testing stimuli of different ultrasound pressures, durations and repetitions rates, the stimuli were presented randomly.
Blinding	Blinding was not performed for transfected and non-transfected groups because the fluorescence of the transgene was used to locate the transfected area for electrophysiological recordings and behavior analysis.

Behavioural & social sciences study design

All studies must disclose on these points even when the disclosure is negative.

Study description	*Briefly describe the study type including whether data are quantitative, qualitative, or mixed-methods (e.g. qualitative cross-sectional, quantitative experimental, mixed-methods case study).*
Research sample	*State the research sample (e.g. Harvard university undergraduates, villagers in rural India) and provide relevant demographic information (e.g. age, sex) and indicate whether the sample is representative. Provide a rationale for the study sample chosen. For studies involving existing datasets, please describe the dataset and source.*
Sampling strategy	*Describe the sampling procedure (e.g. random, snowball, stratified, convenience). Describe the statistical methods that were used to predetermine sample size OR if no sample-size calculation was performed, describe how sample sizes were chosen and provide a rationale for why these sample sizes are sufficient. For qualitative data, please indicate whether data saturation was considered, and what criteria were used to decide that no further sampling was needed.*

Data collection	*Provide details about the data collection procedure, including the instruments or devices used to record the data (e.g. pen and paper, computer, eye tracker, video or audio equipment) whether anyone was present besides the participant(s) and the researcher, and whether the researcher was blind to experimental condition and/or the study hypothesis during data collection.*
Timing	*Indicate the start and stop dates of data collection. If there is a gap between collection periods, state the dates for each sample cohort.*
Data exclusions	*If no data were excluded from the analyses, state so OR if data were excluded, provide the exact number of exclusions and the rationale behind them, indicating whether exclusion criteria were pre-established.*
Non-participation	*State how many participants dropped out/declined participation and the reason(s) given OR provide response rate OR state that no participants dropped out/declined participation.*
Randomization	*If participants were not allocated into experimental groups, state so OR describe how participants were allocated to groups, and if allocation was not random, describe how covariates were controlled.*

Ecological, evolutionary & environmental sciences study design

All studies must disclose on these points even when the disclosure is negative.

Study description	*Briefly describe the study. For quantitative data include treatment factors and interactions, design structure (e.g. factorial, nested, hierarchical), nature and number of experimental units and replicates.*
Research sample	*Describe the research sample (e.g. a group of tagged Passer domesticus, all Stenocereus thurberi within Organ Pipe Cactus National Monument), and provide a rationale for the sample choice. When relevant, describe the organism taxa, source, sex, age range and any manipulations. State what population the sample is meant to represent when applicable. For studies involving existing datasets, describe the data and its source.*
Sampling strategy	*Note the sampling procedure. Describe the statistical methods that were used to predetermine sample size OR if no sample-size calculation was performed, describe how sample sizes were chosen and provide a rationale for why these sample sizes are sufficient.*
Data collection	*Describe the data collection procedure, including who recorded the data and how.*
Timing and spatial scale	*Indicate the start and stop dates of data collection, noting the frequency and periodicity of sampling and providing a rationale for these choices. If there is a gap between collection periods, state the dates for each sample cohort. Specify the spatial scale from which the data are taken*
Data exclusions	*If no data were excluded from the analyses, state so OR if data were excluded, describe the exclusions and the rationale behind them, indicating whether exclusion criteria were pre-established.*
Reproducibility	*Describe the measures taken to verify the reproducibility of experimental findings. For each experiment, note whether any attempts to repeat the experiment failed OR state that all attempts to repeat the experiment were successful.*
Randomization	*Describe how samples/organisms/participants were allocated into groups. If allocation was not random, describe how covariates were controlled. If this is not relevant to your study, explain why.*
Blinding	*Describe the extent of blinding used during data acquisition and analysis. If blinding was not possible, describe why OR explain why blinding was not relevant to your study.*

Did the study involve field work? ☐ Yes ☐ No

Field work, collection and transport

Field conditions	*Describe the study conditions for field work, providing relevant parameters (e.g. temperature, rainfall).*
Location	*State the location of the sampling or experiment, providing relevant parameters (e.g. latitude and longitude, elevation, water depth).*
Access & import/export	*Describe the efforts you have made to access habitats and to collect and import/export your samples in a responsible manner and in compliance with local, national and international laws, noting any permits that were obtained (give the name of the issuing authority, the date of issue, and any identifying information).*
Disturbance	*Describe any disturbance caused by the study and how it was minimized.*

Reporting for specific materials, systems and methods

We require information from authors about some types of materials, experimental systems and methods used in many studies. Here, indicate whether each material, system or method listed is relevant to your study. If you are not sure if a list item applies to your research, read the appropriate section before selecting a response.

Materials & experimental systems

n/a	Involved in the study
☐	☒ Antibodies
☒	☐ Eukaryotic cell lines
☒	☐ Palaeontology and archaeology
☐	☒ Animals and other organisms
☒	☐ Clinical data
☒	☐ Dual use research of concern

Methods

n/a	Involved in the study
☒	☐ ChIP-seq
☒	☐ Flow cytometry
☒	☐ MRI-based neuroimaging

Antibodies

Antibodies used: Polyclonal RBPMS antibodies, NeuN antibody clone 60, polyclonal alexa Flupr secondary antibodies.

Validation: The RNA binding protein RBPMS is a selective marker of ganglion cells in the mammalian retina.
Rodriguez, AR; de Sevilla Müller, LP; Brecha, NC
The Journal of comparative neurology 522 1411-43 2014. Manufacter garantees reactivity in rats and Immunofluorescence application of the antibody.
Anti-NeuN Antibody, clone A60 detects level of NeuN and has been published and validated for use in Immunofluorescence in rats. The antibody specifically recognizes the DNA-binding, neuron-specific protein NeuN, which is present in most CNS and PNS neuronal cell types of all vertebrates tested.

Eukaryotic cell lines

Policy information about cell lines and Sex and Gender in Research

Cell line source(s): *State the source of each cell line used and the sex of all primary cell lines and cells derived from human participants or vertebrate models.*

Authentication: *Describe the authentication procedures for each cell line used OR declare that none of the cell lines used were authenticated.*

Mycoplasma contamination: *Confirm that all cell lines tested negative for mycoplasma contamination OR describe the results of the testing for mycoplasma contamination OR declare that the cell lines were not tested for mycoplasma contamination.*

Commonly misidentified lines (See ICLAC register): *Name any commonly misidentified cell lines used in the study and provide a rationale for their use.*

Palaeontology and Archaeology

Specimen provenance: *Provide provenance information for specimens and describe permits that were obtained for the work (including the name of the issuing authority, the date of issue, and any identifying information). Permits should encompass collection and, where applicable, export.*

Specimen deposition: *Indicate where the specimens have been deposited to permit free access by other researchers.*

Dating methods: *If new dates are provided, describe how they were obtained (e.g. collection, storage, sample pretreatment and measurement), where they were obtained (i.e. lab name), the calibration program and the protocol for quality assurance OR state that no new dates are provided.*

☐ Tick this box to confirm that the raw and calibrated dates are available in the paper or in Supplementary Information.

Ethics oversight: *Identify the organization(s) that approved or provided guidance on the study protocol, OR state that no ethical approval or guidance was required and explain why not.*

Note that full information on the approval of the study protocol must also be provided in the manuscript.

Animals and other research organisms

Policy information about studies involving animals; ARRIVE guidelines recommended for reporting animal research, and Sex and Gender in Research

Laboratory animals	Male C57BL/6J mice aged 9 weeks Male P23H rats (9-22 months), Male Long evans rats 2-12 months
Wild animals	no
Reporting on sex	Experiments were done on male for ease of housing. No sex difference is expected in the experiments
Field-collected samples	no
Ethics oversight	The experimental protocol was approved by the Local Animal Ethics Committee (Committee Charles Darwin n°5, registration number : 9529 and 26889).

Note that full information on the approval of the study protocol must also be provided in the manuscript.

Clinical data

Policy information about clinical studies

All manuscripts should comply with the ICMJE guidelines for publication of clinical research and a completed CONSORT checklist must be included with all submissions.

Clinical trial registration	*Provide the trial registration number from ClinicalTrials.gov or an equivalent agency.*
Study protocol	*Note where the full trial protocol can be accessed OR if not available, explain why.*
Data collection	*Describe the settings and locales of data collection, noting the time periods of recruitment and data collection.*
Outcomes	*Describe how you pre-defined primary and secondary outcome measures and how you assessed these measures.*

Dual use research of concern

Policy information about dual use research of concern

Hazards

Could the accidental, deliberate or reckless misuse of agents or technologies generated in the work, or the application of information presented in the manuscript, pose a threat to:

No	Yes	
☐	☐	Public health
☐	☐	National security
☐	☐	Crops and/or livestock
☐	☐	Ecosystems
☐	☐	Any other significant area

Experiments of concern

Does the work involve any of these experiments of concern:

No	Yes	
☐	☐	Demonstrate how to render a vaccine ineffective
☐	☐	Confer resistance to therapeutically useful antibiotics or antiviral agents
☐	☐	Enhance the virulence of a pathogen or render a nonpathogen virulent
☐	☐	Increase transmissibility of a pathogen
☐	☐	Alter the host range of a pathogen
☐	☐	Enable evasion of diagnostic/detection modalities
☐	☐	Enable the weaponization of a biological agent or toxin
☐	☐	Any other potentially harmful combination of experiments and agents

ChIP-seq

Data deposition

☐ Confirm that both raw and final processed data have been deposited in a public database such as GEO.

☐ Confirm that you have deposited or provided access to graph files (e.g. BED files) for the called peaks.

Data access links *May remain private before publication.*	*For "Initial submission" or "Revised version" documents, provide reviewer access links. For your "Final submission" document, provide a link to the deposited data.*
Files in database submission	*Provide a list of all files available in the database submission.*
Genome browser session (e.g. UCSC)	*Provide a link to an anonymized genome browser session for "Initial submission" and "Revised version" documents only, to enable peer review. Write "no longer applicable" for "Final submission" documents.*

Methodology

Replicates	*Describe the experimental replicates, specifying number, type and replicate agreement.*
Sequencing depth	*Describe the sequencing depth for each experiment, providing the total number of reads, uniquely mapped reads, length of reads and whether they were paired- or single-end.*
Antibodies	*Describe the antibodies used for the ChIP-seq experiments; as applicable, provide supplier name, catalog number, clone name, and lot number.*
Peak calling parameters	*Specify the command line program and parameters used for read mapping and peak calling, including the ChIP, control and index files used.*
Data quality	*Describe the methods used to ensure data quality in full detail, including how many peaks are at FDR 5% and above 5-fold enrichment.*
Software	*Describe the software used to collect and analyze the ChIP-seq data. For custom code that has been deposited into a community repository, provide accession details.*

Flow Cytometry

Plots

Confirm that:

☐ The axis labels state the marker and fluorochrome used (e.g. CD4-FITC).

☐ The axis scales are clearly visible. Include numbers along axes only for bottom left plot of group (a 'group' is an analysis of identical markers).

☐ All plots are contour plots with outliers or pseudocolor plots.

☐ A numerical value for number of cells or percentage (with statistics) is provided.

Methodology

Sample preparation	*Describe the sample preparation, detailing the biological source of the cells and any tissue processing steps used.*
Instrument	*Identify the instrument used for data collection, specifying make and model number.*
Software	*Describe the software used to collect and analyze the flow cytometry data. For custom code that has been deposited into a community repository, provide accession details.*
Cell population abundance	*Describe the abundance of the relevant cell populations within post-sort fractions, providing details on the purity of the samples and how it was determined.*
Gating strategy	*Describe the gating strategy used for all relevant experiments, specifying the preliminary FSC/SSC gates of the starting cell population, indicating where boundaries between "positive" and "negative" staining cell populations are defined.*

☐ Tick this box to confirm that a figure exemplifying the gating strategy is provided in the Supplementary Information.

Magnetic resonance imaging

Experimental design

Design type	*Indicate task or resting state; event-related or block design.*

Design specifications

Specify the number of blocks, trials or experimental units per session and/or subject, and specify the length of each trial or block (if trials are blocked) and interval between trials.

Behavioral performance measures

State number and/or type of variables recorded (e.g. correct button press, response time) and what statistics were used to establish that the subjects were performing the task as expected (e.g. mean, range, and/or standard deviation across subjects).

Acquisition

Imaging type(s)

Specify: functional, structural, diffusion, perfusion.

Field strength

Specify in Tesla

Sequence & imaging parameters

Specify the pulse sequence type (gradient echo, spin echo, etc.), imaging type (EPI, spiral, etc.), field of view, matrix size, slice thickness, orientation and TE/TR/flip angle.

Area of acquisition

State whether a whole brain scan was used OR define the area of acquisition, describing how the region was determined.

Diffusion MRI ☐ Used ☐ Not used

Preprocessing

Preprocessing software

Provide detail on software version and revision number and on specific parameters (model/functions, brain extraction, segmentation, smoothing kernel size, etc.).

Normalization

If data were normalized/standardized, describe the approach(es): specify linear or non-linear and define image types used for transformation OR indicate that data were not normalized and explain rationale for lack of normalization.

Normalization template

Describe the template used for normalization/transformation, specifying subject space or group standardized space (e.g. original Talairach, MNI305, ICBM152) OR indicate that the data were not normalized.

Noise and artifact removal

Describe your procedure(s) for artifact and structured noise removal, specifying motion parameters, tissue signals and physiological signals (heart rate, respiration).

Volume censoring

Define your software and/or method and criteria for volume censoring, and state the extent of such censoring.

Statistical modeling & inference

Model type and settings

Specify type (mass univariate, multivariate, RSA, predictive, etc.) and describe essential details of the model at the first and second levels (e.g. fixed, random or mixed effects; drift or auto-correlation).

Effect(s) tested

Define precise effect in terms of the task or stimulus conditions instead of psychological concepts and indicate whether ANOVA or factorial designs were used.

Specify type of analysis: ☐ Whole brain ☐ ROI-based ☐ Both

Statistic type for inference (See Eklund et al. 2016)

Specify voxel-wise or cluster-wise and report all relevant parameters for cluster-wise methods.

Correction

Describe the type of correction and how it is obtained for multiple comparisons (e.g. FWE, FDR, permutation or Monte Carlo).

Models & analysis

n/a	Involved in the study
☐	☐ Functional and/or effective connectivity
☐	☐ Graph analysis
☐	☐ Multivariate modeling or predictive analysis

Functional and/or effective connectivity

Report the measures of dependence used and the model details (e.g. Pearson correlation, partial correlation, mutual information).

Graph analysis

Report the dependent variable and connectivity measure, specifying weighted graph or binarized graph, subject- or group-level, and the global and/or node summaries used (e.g. clustering coefficient, efficiency, etc.).

Multivariate modeling and predictive analysis

Specify independent variables, features extraction and dimension reduction, model, training and evaluation metrics.